

Experimental and computational analysis of the thermal degradation and the loss of strength of engineered wood-based panels

*Wickramasooriyage Devmini Maheshani
Kularatne*

**Fire Safety Engineering
Lund University
Sweden**

Report 5672, Lund 2022

Master Thesis in Fire Safety Engineering



Experimental and computational analysis of the thermal degradation and the loss of strength of engineered wood-based panels

Wickramasooriyage Devmini Maheshani Kularatne

Report 5672

ISRN: LUTVDG/TVBB—5672-SE

Number of pages: 72

Illustrations: 55

Keywords

Oriented strand board, thermal decomposition, mechanical degradation, heat transfer modelling

Abstract

The current trends in the construction industry push toward materials that are more sustainable and environmentally friendlier than more traditional building materials such as concrete and steel. Timber and timber composites are one of the most popular materials on this list, due to both their mechanical strength and pleasant aesthetics. Oriented strand board (OSB) is one of these timber composites gaining traction in the construction field due to its low cost and sustainable use of timber products in manufacturing.

The major barrier to the effective use of OSB panels in construction is their susceptibility to fire and high thermal conditions. The impact of high thermal conditions on the mechanical strength of OSB must be quantified, so that accurate predictions can be made. This would allow the timber composite manufacturing industries to develop thermal and fire-retardant solutions to improve the thermal-mechanical behavior of OSB.

The goal of this research work was to gain an understanding of the thermal degradation of OSB and its relative impact on the behavior of thermal material properties and mechanical degradation. The scope of the research was limited to pre-ignition behavior. The work in this thesis was split into three major parts. First, a series of thermal material property tests (TGA, thermal conductivity, and cone calorimeter tests) were performed to gain an understanding of the thermal degradation of the OSB. Second, a series of thermal-mechanical combination experiments were conducted to identify a trend between thermal -decomposition and mechanical degradation of OSB. Finally, a heat transfer model based on the cone calorimeter test was simulated and compared with results from experimental measurements.

Major findings from the research work include the trend of thermal degradation of OSB. Until a temperature of 225 °C, the mass loss is minimal (1.9 ± 0.1 %) after which, a large mass loss of a further 66% is observed by the temperature range 380 ± 10 °C. Another finding is regarding the thermal decomposition-mechanical degradation behavior of OSB. The failure stress trend associated with thermal degradation was found to be different for specimens tested immediately after removing from the furnace and for specimens tested after a 24-hour period of cooling. For specimens tested immediately after removal from the furnace, the failure stress had a continuous, non-linear degradation from room temperature to 200 °C. However, for the specimens allowed to cool for 24 hours, an upward trend was observed between 75 ° and 100 °C for the failure stress. For the specimens tested at 100 °C, 150 °C, 175 °C, and 200 °C, it was also found that the 24-hour cooling period allowed strength to be regained in the OSB.

© Copyright: Fire Safety Engineering, Lund University
Lund 2022.

Fire Safety Engineering
Lund University
P.O. Box 118
SE-221 00 Lund
Sweden

<http://www.brand.lth.se>

Telephone: +46 46 222 73 60



HOST UNIVERSITY: Lund University

FACULTY: Faculty of Engineering

DEPARTMENT: Division of Fire Safety Engineering

Academic Year 2021-2022

**EXPERIMENTAL AND COMPUTATIONAL ANALYSIS OF THE THERMAL
DEGRADATION AND THE LOSS OF STRENGTH OF ENGINEERED WOOD-
BASED PANELS**

Wickramasooriyage Devmini Maheshani Kularatne

Promoter: Margaret McNamee, Lund University

Master thesis submitted in the Erasmus Mundus Study Programme

International Master of Science in Fire Safety Engineering

Disclaimer

This thesis is submitted in partial fulfilment of the requirements for the degree of *The International Master of Science in Fire Safety Engineering (IMFSE)*. This thesis has never been submitted for any degree or examination to any other University/programme. The author declares that this thesis is original work except where stated. This declaration constitutes an assertion that full and accurate references and citations have been included for all material, directly included and indirectly contributing to the thesis. The author(s) gives (give) permission to make this master thesis available for consultation and to copy parts of this master thesis for personal use. In the case of any other use, the limitations of the copyright must be respected, in particular with regard to the obligation to state expressly the source when quoting results from this master thesis. The thesis supervisor must be informed when data or results are used.

Read and approved.

Wickramasooriyage Devmini Maheshani Kularatne

10th of May 2022

Abstract

The current trends in the construction industry push toward materials that are more sustainable and environmentally friendlier than more traditional building materials such as concrete and steel. Timber and timber composites are one of the most popular materials on this list, due to both their mechanical strength and pleasant aesthetics. Oriented strand board (OSB) is one of these timber composites gaining traction in the construction field due to its low cost and sustainable use of timber products in manufacturing.

The major barrier to the effective use of OSB panels in construction is their susceptibility to fire and high thermal conditions. The impact of high thermal conditions on the mechanical strength of OSB must be quantified, so that accurate predictions can be made. This would allow the timber composite manufacturing industries to develop thermal and fire-retardant solutions to improve the thermal-mechanical behavior of OSB.

The goal of this research work was to gain an understanding of the thermal degradation of OSB and its relative impact on the behavior of thermal material properties and mechanical degradation. The scope of the research was limited to pre-ignition behavior. The work in this thesis was split into three major parts. First, a series of thermal material property tests (TGA, thermal conductivity, and cone calorimeter tests) were performed to gain an understanding of the thermal degradation of the OSB. Second, a series of thermal-mechanical combination experiments were conducted to identify a trend between thermal -decomposition and mechanical degradation of OSB. Finally, a heat transfer model based on the cone calorimeter test was simulated and compared with results from experimental measurements.

Major findings from the research work include the trend of thermal degradation of OSB. Until a temperature of 225 °C, the mass loss is minimal (1.9 ± 0.1 %) after which, a large mass loss of a further 66% is observed by the temperature range 380 ± 10 °C. Another finding is regarding the thermal decomposition-mechanical degradation behavior of OSB. The failure stress trend associated with thermal degradation was found to be different for specimens tested immediately after removing from the furnace and for specimens tested after a 24-hour period of cooling. For specimens tested immediately after removal from the furnace, the failure stress had a continuous, non-linear degradation from room temperature to 200 °C. However, for the specimens allowed to cool for 24 hours, an upward trend was observed between 75 ° and 100 °C for the failure stress. For the specimens tested at 100 °C, 150 °C, 175 °C, and 200 °C, it was also found that the 24-hour cooling period allowed strength to be regained in the OSB.

සාරාංශය (Abstract in Sinhalese)

ඉදිකිරීම් ක්ෂේත්‍රයේ නව ප්‍රවණතාවන්ට අනුව, කොන්ක්‍රීට් හා යකඩ වැනි සාම්ප්‍රදායික ද්‍රව්‍යවලට වඩා තිරසාර හා පරිසර හිතකාමී ද්‍රව්‍ය භාවිතා කිරීම දිරිමත් කෙරේ. එවන් ද්‍රව්‍ය අතර දැව හා දැව සංයුක්ත සඳහා ප්‍රමුඛස්ථානයක් ලැබෙන අතර, ඒ සඳහා දැවවල ඇති ආකර්ශනීය පෙනුම හා ශක්තිමත් බව බලපා ඇත. ඔරියන්ටඩ් ස්ට්‍රැන්ඩ් බෝඩ් (ඕ.එස්.බී.) යනු එවැනි දැව සංයුක්තයක් වන අතර ඒවා එහි ලාභදායී බව හා නිෂ්පාදන ක්‍රියාවලීන්ගේදී සිදු කරන තිරසාර භාවිතය නිසා ඉදිකිරීම් ක්ෂේත්‍රය තුළ ඉහළ ආකර්ෂණයක් අත් කර ගනිමින් පවතී.

ඕ.එස්.බී. පැහල ස්ඵලදායීව භාවිතා කිරීම සඳහා පවතින ප්‍රධානම ගැටළුව වන්නේ ඒවායේ ඇති ගිනි ගැනීමේ හැකියාව හා අධික උෂ්ණත්වවලට නිරාවරණය වීමේ හැකියාවන්ය. අධික උෂ්ණත්වයන් හමුවේ ඕඑස්බී පැහලවල යාන්ත්‍රික ශක්තියට ඇතිවන බලපෑම ප්‍රාමාණීකරණය කළ යුතු අතර, එමගින් ඒ සම්බන්ධව නිවැරදි පුරෝකථනයන් කිරීමට හැකියාව ලැබෙනු ඇත. එමගින් නිෂ්පාදන කාර්යක්ෂමතාවන් හට ගිනි හා තාප ප්‍රතිරෝධී විසඳුම් සොයාගැනීම තුළින් ඕඑස්බීවල තාප-යාන්ත්‍රික හැසිරීම වැඩිදියුණු කර ගැනීමට අවස්ථාව හිමි වනු ඇත.

මෙම පර්යේෂණයේ අරමුණ වූයේ ඕ.එස්.බී. වල තාප-භායනිය සම්බන්ධ අවබෝධයක් ලබා ගැනීම හා එමගින් ද්‍රව්‍යයේ තාප-ලක්ෂණ හා යාන්ත්‍රික-භායනිය සඳහා ඇති කරන ලද සාපේක්ෂ බලපෑම සම්බන්ධ අවබෝධයක් ලබා ගැනීමයි. පර්යේෂණයේ විෂය පථය, දැනනය වීමට ප්‍රථමව හැසිරීම අධ්‍යයනය කිරීමට සීමා කරන ලදී. මෙම නිබන්ධනයේ ඇති කාර්යයන් වර්ග 3කට බෙදා දැක්විය හැකිය. පළමුව, ඕ.එස්.බී. හි තාප භායනිය සිදු වන අයුරු අවබෝධ කර ගැනීම සඳහා තාප-ලක්ෂණ පරීක්ෂණ පෙළක් (TGA, තාප සන්නායකතා හා කෝන් කැලරිමීටර් පරීක්ෂණ) සිදු කරන ලදී. දෙවනුව, තාප-වියෝජනය හා යාන්ත්‍රික-භායනිය අතර සම්බන්ධයක් හඳුනාගැනීම සඳහා තාප-යාන්ත්‍රික සංයුක්ත පරීක්ෂණ පෙළක් සිදු කරන ලදී. අවසන් වශයෙන්, කෝන් කැලරිමීටර් පරීක්ෂණය පාදක කර ගත් තාප හුවමාරු ආකෘතියක් (මොඩලයක්) ආදර්ශනය කර එහි ප්‍රතිඵල, පරීක්ෂණවලින් ලබා ගත් ප්‍රතිඵල සමග සංසන්දනය කරන ලදී.

ඕ.එස්.බී. වල තාප-භායනියට ඇති හැඹුරුතාව ප්‍රාමාණීකරණය, පර්යේෂණයේ ප්‍රධානතම ප්‍රතිඵල අතරින් එකකි. 225 °C දක්වා ස්කන්ධ හානිය අවම (1.9 ± 0.1 %) වන නමුත්, උෂ්ණත්වය 380 ± 10 °C පරාසයට පැමිණි විටදී 66% ක විශාල ස්කන්ධ හානියක් සිදු වේ. තවත් ප්‍රතිඵලයක් සම්බන්ධ වන්නේ ඕ.එස්.බී. වල තාප-වියෝජනයට හා යාන්ත්‍රික-භායනිය අතර සම්බන්ධයටය. තාප භායනියට සම්බන්ධ විනාශ වීමේ ප්‍රත්‍යාබලය, උදුනෙන් ඉවත් කළ විගස පරීක්ෂා කළ නිදර්ශකයන්ට වඩා වෙනස් අගයක්, පැය 24ක් සිසිල් වීමට ඉඩ හැර පරීක්ෂා කළ නිදර්ශකයන් පෙන්නුම් කරන ලදී. උදුනෙන් ඉවත් කළ විගස පරීක්ෂා කළ නිදර්ශකයන්ගේ විනාශ වීමේ ප්‍රත්‍යාබලය කාමර උෂ්ණත්වයේ සිට 200 °C දක්වා සන්තතික හා රේඛීය නොවන භායනියක් පෙන්නුම් කරන ලදී. නමුත් පැය 24ක් සිසිල් වීමට ඉඩ හැර පරීක්ෂා කළ නිදර්ශකයන්ගේ විනාශ වීමේ ප්‍රත්‍යාබලය සඳහා 75 °C සිට 100 °C දක්වා උඩු අතට යන හැඹුරුවක් නිරීක්ෂණය කරන ලදී. එසේම 100 °C, 150 °C, 175 °C, හා 200 °C හිදී පරීක්ෂා කරන ලද නිදර්ශකයන් පැය 24ක් සිසිල් වීමට ඉඩ ලබා දුන් විටදී ඒවායේ ශක්තිය ප්‍රතිසංස්ථාපනය වන බවද නිරීක්ෂණය කරන ලදී.

Acknowledgements

I would like to express my gratitude to several individuals without whose help this work would not have been completed.

My heartfelt thanks go to my supervisors during my thesis work, Margaret McNamee, Blanca Andres, Ana Sauca and Karlis Livkiss for their advice and guidance during the research work and thesis writing.

I would also like to thank the Dansk Brand- og Sikringsteknisk Institut (DBI) for the provision of equipment and materials to perform the planned experiments. I'm also grateful to the staff of DBI, especially Abhishek Bhargava, Alexandru Radulescu Ian Pope, and Bjarne Husted for their help with performing the tests as well as the expertise they provided regarding the research work.

Last, but not least, I thank my professors and peers at the IMFSE program, who were with me for the past 2 years for their help and support.

Table of Contents

List of Abbreviations	viii
List of Tables	ix
List of Figures	x
Nomenclature	xii
1 Introduction and Objectives	1
1.1 Background	1
1.2 Purpose and Objectives	2
1.3 Hypothesis	3
1.4 Thesis Disposition	3
1.5 Limitations	4
2 Literature Review	5
2.1 Methodology	5
2.2 Engineered Timber	6
2.3 Oriented Strand Board	7
2.3.1 Production Process	7
2.3.2 Classifications of OSB	9
2.4 Thermal Property Tests	9
2.4.1 Cone Calorimeter Tests	9
2.4.2 Thermogravimetric Analysis (TGA)	10
2.4.3 Thermal Conductivity Test	12
2.5 Effect of Moisture Content on Thermal Properties of OSB	13
2.6 Mechanical Performance of OSB	14
2.7 Experiments Linking Mechanical Strength of OSB with Thermal Conditions	16
3 Experimental Methodology	18
3.1 Specimen Specifications	18
3.2 Thermal Property Tests	18
3.2.1 Thermal Conductivity Test	18
3.2.2 TGA Test	18
3.2.3 Cone Calorimeter Test	19
3.3 Thermal-Mechanical Test	20
3.3.1 Equipment	20
3.3.2 Specimen Preparation	21

3.3.3	Heating OSB Samples.....	21
3.3.4	Three-Point Bending Test.....	21
4	Experimental Results	22
4.1	Thermal Property Tests	22
4.1.1	Thermal Conductivity Test	22
4.1.2	TGA Test	23
4.1.3	Cone Calorimeter Test	25
4.2	Thermal-Mechanical Tests.....	29
4.2.1	Temperature Measurements.....	29
4.2.2	Visual Analysis and Mass Loss of Thermal Condition Impact	29
4.2.3	Three-Point Bending Test.....	30
5	Thermal Modelling Methodology.....	34
5.1	Geometry and Heat Flux Boundary Condition	34
5.2	Material Data.....	35
5.3	Simulation Settings	36
6	Thermal Modelling Results.....	37
6.1	Simulation Scenarios with Input of Heat Flux Boundary Condition	37
6.2	Simulation Scenarios with Input of Prescribed Temperature Boundary Condition..	38
6.3	Comparison of Simulation Results with Experimental Measurements.....	38
7	Discussion.....	41
7.1	Thermal Decomposition of OSB.....	41
7.2	Thermal Properties of OSB	41
7.2.1	Thermal Conductivity	42
7.2.2	Cone Calorimeter Tests.....	42
7.3	Thermal Decomposition and Mechanical Degradation of OSB.....	44
7.4	Variations between Heat Transfer Simulation Results and Cone Calorimeter Experimental Measurements.....	46
7.5	Barriers to Comparison of Results	48
8	Summary and Conclusions	49
9	Further Research	51
10	References.....	52
11	Appendices.....	55
11.1	Declaration of Performance of the Testing Specimen.....	55

List of Abbreviations

CHF	Critical heat flux
CLT	Cross Laminated Timber
DSC	Differential Scanning Calorimeter
GLT	Glue Laminated Timber
HRR	Heat release rate
MCC	Microscale Combustion Calorimeter
MC	Moisture content
MOR	Modulus of rupture
OSB	Oriented Strand Board
RT	Room temperature
TGA	Thermogravimetric Analysis

List of Tables

Table 1: Cone calorimeter test results of White and Winandy (2006)	9
Table 2: Cone calorimeter test results of Rantuch et al. (2015).....	10
Table 3: Cone calorimeter test average results of Ira et al. (2020)	10
Table 4: Results from past TGA tests	11
Table 5: Summarization of compression and tensile tests of Chen and He (2017)	15
Table 6: Stress-strain graphs for the experimental results of Chen and He (2017)	15
Table 7: Reduction of mass and bending strength of OSB at different temperature levels	17
Table 8: Thermal conductivity test readings.....	22
Table 9: Calculated mass loss (%) from TGA results.....	25
Table 10: Ignition temperature for each cone calorimeter test	27
Table 11: Peak HRR, time to reach peak HRR and average effective heat of combustion.....	28
Table 12: Average mass loss at each temperature level	30
Table 13: Average values for strength regained at 24 hours of cooling in the thermal-mechanical tests	33
Table 14: Material properties of ceramic wool.....	35
Table 15: <i>HRR_{peak}</i> value comparison between experimental and literature results	43
Table 16: <i>tig</i> value comparison between experimental and literature results.....	43

List of Figures

Figure 1: Methodology used in the literature review	5
Figure 2: Cross laminated timber.....	7
Figure 3: Glue laminated timber	7
Figure 4: Plywood.....	7
Figure 5: Chipboard	7
Figure 6: Oriented strand board	8
Figure 7: Strand types in OSB	8
Figure 8: The manufacturing process of OSB	8
Figure 9: Results of thermal conductivity test by Sonderegger and Niemz (2009).....	13
Figure 10: Thermal conductivity of OSB versus temperature by Vololonirina et al. (2014) ..	13
Figure 11: Effect of moisture content on thermal properties of OSB	13
Figure 12: Cutting patterns of specimens	14
Figure 13: Specimens for compression and tensile tests respectively	14
Figure 14: Four-point bending test ($a = L/3$)	16
Figure 15: Summary of the bending tests for OSB by Sinha et al. (2011)	16
Figure 16: Summary of thermal-mechanical tests for OSB by Bekhta et al. (2003).....	17
Figure 17: Set-up of the cone-calorimeter apparatus	19
Figure 18: Setup of the OSB3 material with the thermocouples in the cone calorimeter test .	19
Figure 19: Furnace used to heat OSB3 samples	20
Figure 20: Three-point bending test rig	20
Figure 21: Attaching thermocouple to the center of OSB3 sample	21
Figure 22: Variation in thermal conductivity coefficient with temperature	23
Figure 23: Variation of mass with temperature in TGA test	24
Figure 24: Variation of mass loss rate with temperature in TGA tests.....	24
Figure 25: OSB3 sample during cone calorimeter test and afterwards	25
Figure 26: Temperature reading for cone calorimeter test (15 kW/m^2).....	26
Figure 27: Temperature reading for cone calorimeter test (25 kW/m^2).....	26
Figure 28: Temperature reading for cone calorimeter test (35 kW/m^2).....	26
Figure 29: Graph of $1/t_{ig}$ vs radiant heat flux in cone calorimeter test.....	27
Figure 30: Heat release rate curves of the cone calorimeter tests.....	28
Figure 31: Variation of temperature with time in OSB3 specimen center in the furnace	29
Figure 32: Time OSB3 samples were kept in furnace in the thermal-mechanical tests	29
Figure 33: Visual of test samples upon removing from the furnace.....	30
Figure 34: Stress-strain graph – Mechanical testing immediately after heating.....	31
Figure 35: Stress-strain graph – Mechanical testing at 24 hours of cooling after heating.....	31
Figure 36: Failure stresses - Mechanical testing immediately after heating.....	32
Figure 37: Failure stresses - Mechanical testing at 24 hours of cooling after heating.....	32
Figure 38: Heat transfer model used for thermal simulation	34
Figure 39: Heat flux boundary condition on the heat transfer model	35
Figure 40: Thermal insulation on the heat transfer model.....	35
Figure 41: Plot of specific heat capacity of OSB3 against temperature	36

Figure 42: Plot of thermal conductivity of OSB3 against temperature	36
Figure 43: Temperature-time curve of top surface from cone calorimeter data	36
Figure 44: Mesh setting in heat transfer model	36
Figure 45: Surface temperature at 1100 s – Simulation scenario 1	37
Figure 46: Temperature-time curves – Simulation scenario 1	37
Figure 47: Surface temperature at 1100 s – Simulation scenario 2	37
Figure 48: Temperature-time curves – Simulation scenario 2.....	37
Figure 49: Surface temperature at 1100 s – Simulation scenario 3	38
Figure 50: Temperature-time curves – Simulation scenario 3.....	38
Figure 51: Comparison of simulation scenario 1 results with experimental measurements....	39
Figure 52: Comparison of simulation scenario 2 results with experimental measurements....	39
Figure 53: Comparison of simulation scenario 3 results with experimental measurements....	40
Figure 54: Comparison of experimental results with results of Bekhta et al. (2003) - Mechanical testing immediately after heating	45
Figure 55: Comparison of experimental results with results of Sinha et al. (2011) - Mechanical testing at 24 hours of cooling after heating.....	45

Nomenclature

A	Area (m ²)
b	Width of test panel (mm)
D	Deflection of the center of the beam (mm)
d	Depth of test panel (mm)
E	Modulus of elasticity (MPa)
HRR_{peak}	First peak heat release rate (kW/m ²)
$\Delta h_{c,eff}$	Effective heat of combustion (J/kg)
h	Convective heat transfer coefficient (W/m ² /K)
k	Thermal conductivity coefficient (W/m/K)
L	Support span (mm)
m_i	Initial mass (kg)
m_f	Final mass (kg)
P	Load at a given point on the load-deflection curve (N)
\dot{Q}	Heat flow (W/m ²)
\dot{q}_i	Instantaneous heat release rate (kW/m ²)
\dot{q}_{rad}''	radiant heat flux (kW/m ²)
\dot{q}_{net}''	Net heat flux on the surface (kW/m ²)
$\dot{q}_{rad,loss}''$	Radiated heat loss (kW/m ²)
\dot{q}_{conv}''	Convective heat loss (kW/m ²)
ΔT	Temperature difference (K)
T_{surf}	Surface temperature (K)
T_{amb}	Ambient temperature (K)
t	Thickness (m)
Δt	Time step (s)
t_{ig}	Time to ignition (s)
t_{peak}	Time to first peak on the HRR curve (s)
σ_b	Stress at midpoint (MPa)
ϵ_b	Strain at midpoint (mm/mm)
ϵ	Emissivity
σ	Stefan-Boltzmann constant

1 Introduction and Objectives

1.1 Background

Timber is considered a valuable material in the construction industry, due to the fact that it can be shaped as needed, has suitable mechanical properties and is aesthetically pleasing. It is also widely promoted as a “Green” material, which is synonymous with sustainable and environmentally friendly. The goal of “Green” or sustainability is to achieve present-day needs without hindering “natural systems, resources, and diversity upon which they are maintained” that will be needed by future generations [1], [2].

Sustainability in construction is a concept consisting of three areas, the “triple bottom line” as it’s termed. First, is environmental stewardship, which means considering the impacts of the development on the natural environment, both positive and negative. The second area is social responsibility, which means considering the impacts on the people involved in the design and development of the project and the people of the community involved in the project. This goal includes creating living and workspaces that are both functional and aesthetically pleasing using materials and products that have been sourced and produced sustainably. The third area is economic prosperity, which considers the economic impact on the project stakeholders [3]. For effective sustainability in a project, all three areas need to be suitably met, reducing the cost and improving the benefits.

Around the world, timber is used as a building material as well as for other purposes in construction including as facades, as a thermal insulating material, and as cladding. However, using timber as is can be disadvantageous due to several reasons. It can be prone to crack, bend, and decay under stresses and natural causes like termite infestations. Natural timber also has a lower durability compared to other construction materials such as steel and concrete. Engineered timber has been developed as a solution to this, having the advantages of timber, but with minimization of the disadvantages.

One such type of engineered timber is Oriented Strand Board (OSB), which is a popular choice for use in residential and commercial timber constructions, packaging, and interior furnishings. The global market for OSB in 2020 was valued at \$10.41 billion, and the expected compound annual growth from 2021 to 2027 is 5.6% [4].

OSB is an evolutionary product from waferboard in the latter part of the 1970s. This timber composite is manufactured using thin timber strands of a uniform thickness, and length and width in a pre-determined dimension range. These strands are placed in a determined orientation with a binding agent [5]. OSB is recognized to have the same uses as plywood by many countries’ building codes including the US and Canada. Although similar to plywood in mechanical properties, OSB has a significantly lower production cost [6].

Considering the requirement for more sustainable materials in the construction industry, OSB could be a good alternative to more traditional building materials. However, the fact that OSB, as a timber composite, is susceptible to high temperatures and fire can be a negative point when choosing it as a more prominent material for the construction industry.

The chemical constituents of wood can experience thermal degradation at raised temperatures that will affect structural performance. When exceeding temperatures of 65°C, the strength and modulus of elasticity can face permanent reductions [7]. Due to the composition of OSB, it is much less resistant to high temperatures than solid wood and could fail comparatively quickly [8], [9].

For a good fire-resistant structural design, it is important that structural integrity is maintained during and after the fire [10]. To use OSB in a structural capacity, it is necessary to first study and identify the fire performance of the OSB material with exposure to high thermal conditions, considering both the mechanical properties and the thermal properties of the material.

The project presented in this thesis includes a thorough literature review of work previously done on this subject. Following this, experimental work was conducted to investigate the tensile and bending strength of OSB at room temperature as well as at elevated temperatures. In parallel, material tests were also performed to obtain thermal properties and performance of the material which were used for thermal modeling of the material. This work was done in support of the purpose and objectives as stated in the next section.

1.2 Purpose and Objectives

Although timber and timber composites are touted as sustainable building materials, they have a lower tolerance to high temperatures compared to more traditional building materials like concrete and steel. This is a barrier to choosing timber composites such as OSB in buildings. In order to facilitate the use of OSB in the construction industry, it is first needed to improve the understanding of its behavior at high temperature and fire conditions. This knowledge can be used to introduce procedures like fire retardants to improve high thermal and fire behavior.

The main purpose of this research is to investigate the fire behavior of OSB panels, especially the relationship between its thermal decomposition in high thermal conditions and the loss of strength at high temperatures.

This research project has three main objectives:

The first objective is to analyze the degradation of OSB with increasing temperature. Considering that the material is composed of two main components, wood chips, and resin, it is to be expected that there may be differences in the degradation pattern between OSB and solid timber. Through a series of thermal material property tests (TGA, cone calorimeter, thermal conductivity test), the changes in OSB with increasing temperature in terms of factors such as mass loss, mass loss rate, and thermal conductivity are identified.

The second objective is to investigate the connection between thermal decomposition and mechanical degradation in OSB through experimental testing. The mechanical strength of the material immediately after exposure to a high thermal condition as well as after a cooling down period after exposure to a high thermal condition is investigated. Through analysis of the data, a relationship between failure stress and the temperature of OSB is obtained.

The third objective is to conduct modelling of heat transfer in OSB. The test procedure used in the cone calorimeter tests was emulated in the thermal modelling and the material was modelled using data obtained from the literature review and the experimental work. The results obtained were compared against the results from the experimental test analysis. Through this, the material data used in the thermal modelling is validated.

1.3 Hypothesis

This research project is based on the hypothesis that OSB is affected by high thermal conditions in terms of chemical and mechanical properties. With increasing temperature, OSB as a timber composite consisting of organic matter, will experience degradation of the material and material bonds. This will cause a correlated decline in the material's mechanical strength. However, it is also hypothesized that this decline may not be temporary up to a certain temperature value and with a cooling off period, a portion of the lost mechanical strength may be regained in the material.

1.4 Thesis Disposition

This section describes the disposition of this thesis.

- 1. Literature Review:** This section describes the literature survey that was carried out regarding past research conducted on the thermal and mechanical behaviour of OSB. Both experimental and modelling-based research shall be conducted. Special attention shall be given to experimental work that combined thermal and mechanical testing of OSB.
- 2. Experimental Methodology and Experimental Results:** These two sections discuss the procedure of the experimental work done for OSB in this project and the results obtained. The tests were of two types. The first type was thermal material tests in order to investigate the chemical decomposition of OSB with increasing temperature, which is the first defined objective. The tests shall include TGA and DSC tests at different heating rates, thermal conductivity tests, and cone calorimeter tests at three different heat flux values.

The second type of tests was subjecting the pre-defined size of OSB panels to thermal exposure and subsequent bending tests. There were four to six tests conducted for each temperature level and the temperature range considered was between ambient temperature and 200°C. A connection was made as to how the thermal degradation affects the mechanical strength of the material. The analysis of this data achieved the second objective.

- 3. Thermal Modelling Methodology and Thermal Modelling Results:** These two sections describe the thermal modelling performed for the OSB material with input data obtained from the literature survey and experimental work that were conducted. The software "COMSOL MULTIPHYSICS" was used to perform heat transfer modelling of OSB. The results of the simulation were compared against the temperature recordings of the cone calorimeter tests. This achieved the third defined objective.

4. **Discussion:** The data gained from both the experimental tests and thermal modelling was analyzed in this section. The analysis gives information on the significant temperature values regarding the chemical decomposition of OSB. The results of the experimental work were also compared against data obtained from the literature study.
5. **Summary and Conclusions:** This section provides a summary account of the thesis work and the major findings.
6. **Further Research:** This section ends the thesis with suggestions for future work regarding developing the understanding of the behavior of OSB at high thermal conditions.

1.5 Limitations

In this study, the OSB material used was limited to one grade of OSB (OSB3), by one manufacturer. This prevents comparison of test results between different parameters, such as different grades of OSB and different manufacturers' specifications.

The study was also limited to the pre-ignition behavior of OSB. The thermal-mechanical combination tests were limited to a temperature range of 20 °C – 200 °C, and only the mechanical strength of the major axis was tested. The behavior of OSB during fire was not studied.

The experimental tests were limited to small scale tests (or microscale tests in the case of TGA tests). The large-scale structural behavior of OSB was not studied.

2 Literature Review

The literature survey was conducted with the purpose of developing a theoretical understanding of OSB. This chapter aims to compile information regarding the chemical and mechanical behavior of OSB under ambient conditions and higher thermal conditions. The findings were used to develop an experimental and computation plan for the following work of this thesis.

2.1 Methodology

The methodology of this literature study is covered here. Figure 1 illustrates the steps taken to identify relevant studies from literature and source the data required to progress with the research work.

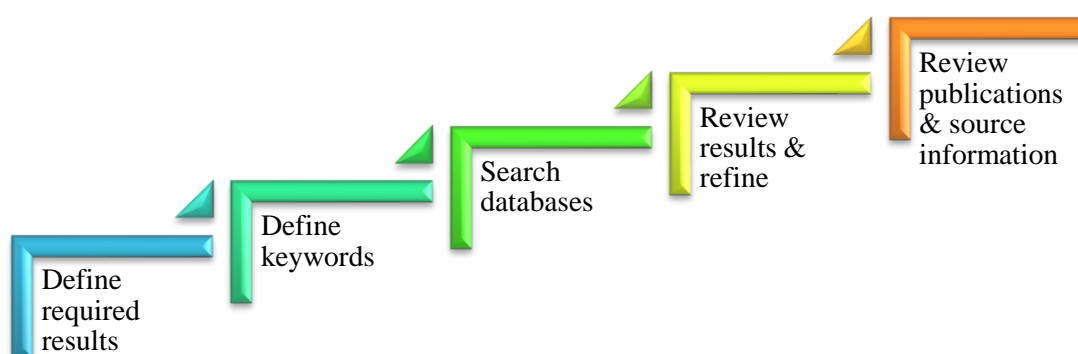


Figure 1: Methodology used in the literature review

First, the pre-defined objectives of the research were used to identify the required results from the research work. These were used as parameters to define the keywords that would be relevant to the research work. The defined keywords are given below.

- Oriented strand board / OSB
- Timber / timber composite
- Thermal property
- Thermal degradation
- Mechanical strength / Modulus of rupture / Failure stress
- Mechanical degradation

Next, the keywords were used to find publications relevant to the research topic in the databases. The following databases were used: LUBsearch (Lund University Library's search engine), ScienceDirect, and Google Scholar.

The studies provided by the database search were further refined first based on the title of the publication and then by the results of the publication. In the refining process, several exclusion criteria were used. Exclusion criteria included articles in languages other than English, studies

focusing only on fire behavior, and studies on timber composites that excluded OSB. For the articles that had the most relevance to the research study, the web tool ResearchRabbit was used to identify other relevant studies that could have been missed in the initial search.

Finally, the refined set of literature studies was reviewed and the information relevant to the was sourced and compiled in section 2.

2.2 Engineered Timber

Due to the limited resources of natural timber of adequate quality and strength, the cost of timber has increased. The high demand for timber along with the dwindling supply of timber and rising costs has been responded with the development of engineered timber such as plywood, laminated veneer lumber, glue-laminated timber and oriented strand board [11]. Engineered wood is typically manufactured by combining wood in the form of boards, strands, sheets or particles.

The typical production process of engineered timber provides several advantages over natural timber [12], e.g.:

- a) Since production is done by combining timber pieces, the wood source is not constrained by the size and smaller trees can also be sourced.
- b) Natural timber contains defects such as knots, that can affect the timber quality. In engineered timber, such defects can be minimized by removing such weak sections of the timber before the manufacturing process.
- c) In natural timber, it is often observed that the material properties can vary along the sections. In engineered timber, the production process can deliver a higher level of consistency, so that material properties along the sections will be similar and predictable.
- d) Natural timber is oriented, i.e., it has a weak axis and a strong axis, which can be a deterrent to its use in structures. This can be avoided in engineered timber by orienting the timber layers in cross-directions, and the strength can be increased.

Engineered timber is a broad term which includes many individual types of timber, developed for different purposes. A few of those are described below.

1. Cross Laminated Timber (CLT)

CLT (Figure 2) is manufactured by stacking an uneven number of timber layers (commonly three, five, or seven layers), arranged crosswise at 90° angles and setting with an adhesive. Each timber layer is composed of timber boards placed parallelly. The laminar property of the panel allows it to support loads in-plane as well as out-of-plane. The manufacturing procedure allows the production of CLT that is both large in terms of the plane and thickness. This, along with its higher strength, can allow the use of CLT as a “stand-alone structural element” [13].

2. Glue Laminated Timber (GLT)

GLT (Figure 3) is produced by stacking timber boards of thickness between 6 mm and 45 mm, setting them with an adhesive. This procedure increases its mechanical strength compared to natural timber, and also allows the production of elements in larger dimensions which are

suitable to be used as structural elements. This engineered timber type can also be manufactured in custom shapes, which is another advantage [14], [15].

3. Plywood

Plywood (Figure 4) is composed of an uneven number of thin timber sheets of thickness between 0.3 mm and 6.3 mm called wood veneers, bound together by an adhesive. The wood veneers are stacked, with consecutive layers placed so that the grain direction of each layer is perpendicular to the layers directly above and below [16]. Plywood is most commonly seen in the construction industry for uses such as exterior wall sheathing, wood panelling, framing interior walls, sheathing roofs and flooring.

4. Chipboard or Particleboard

Chipboard (Figure 5) is produced using wood shavings or wood chips, set using a urea-formaldehyde adhesive and pressed at high temperature and pressure. Popular uses of chipboard are for flooring, ceilings, partitions, and furniture [17].



Figure 2: Cross laminated timber



Figure 3: Glue laminated timber



Figure 4: Plywood



Figure 5: Chipboard

The focus of this thesis, however, is OSB. It will be described in more detail in the next sections.

2.3 Oriented Strand Board

2.3.1 Production Process

OSB (Figure 6) is produced by bonding long wood strands with waterproof and heat-cured synthetic resin-based adhesives. An OSB panel will usually contain layers in three cross-directions. The top and bottom layers are oriented longitudinally while the core layers are oriented perpendicularly [5]. This method of orientation of the timber strands will negate the weak axis in natural timber and thereby improves the mechanical properties of the panel such

as bending strength and stiffness[18], [19]. The strands used for OSB vary in size with a range of 15-25 mm width, 75-150 mm length, and 0.3-0.7 mm thickness as shown in Figure 7 [20].



Figure 6: Oriented strand board



Figure 7: Strand types in OSB
Reproduced from [20] with the permission from Elsevier

The most commonly used resins in the production of wood composites including OSB are phenol-based resins such as urea-formaldehyde and phenol-formaldehyde. These resins provide high-strength, long-lasting bonds in wood composites. The adhesive ratio is one of the most important parameters that affect the properties of OSB. The ratio is usually between 3% to 8%. The experimental work done by Gunduz et al (2011) revealed that by increasing the adhesive ratio from 3% to 6%, the modulus of rupture of OSB increased from the range of 25.3 N/mm² – 30.5 N/mm² to the range of 33.73 N/mm² – 42.27 N/mm² in the flexure parallel [21].

Two of the most important parameters in the production process are adhesive ratio and pressing time. These factors can affect the mechanical and physical properties of the OSB. For panels used for load-bearing applications, it is recommended that the minimum value for adhesive ration and pressing time be 6% and 5 minutes respectively [21].

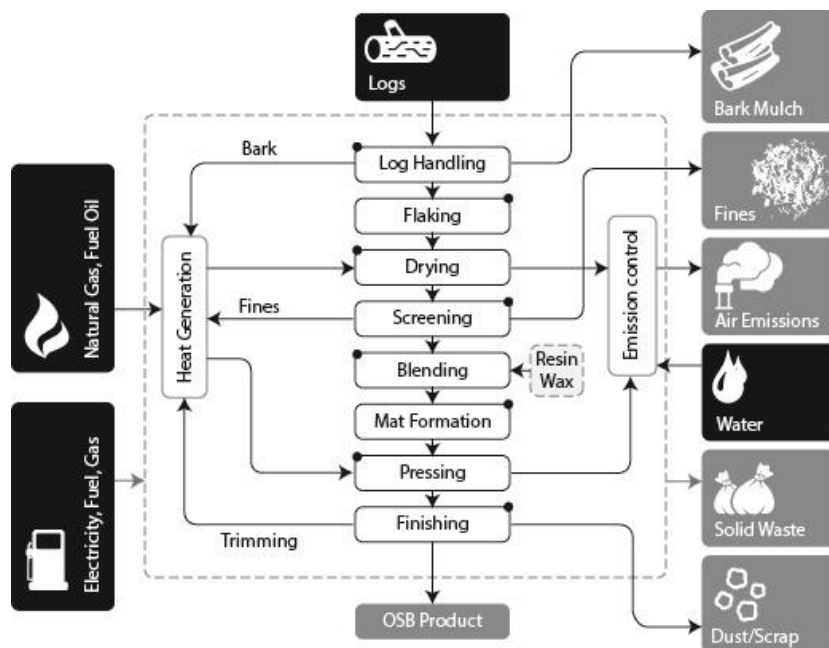


Figure 8: The manufacturing process of OSB
Redrawn from [5]

The complete production process has been described by Kline (2005) as shown by Figure 8 [5]. The process consists of six sub-unit processes. The first four sub-unit processes are log handling and flaking, drying and screening of the timber flakes, blending the timber strands with the adhesives and pressing, and finishing of the panels including cutting to size, sanding and packing. The other two sub-unit processes are regarding the heat generation for the OSB production and control of emissions that occur during the production process including treating harmful emissions prior to releasing them into the environment.

2.3.2 Classifications of OSB

The European standard EN 300 [22] defines 4 grades of OSB, based on structural use.

- OSB1 – For general applications, equipment and interior furniture in a dry environment
- OSB2 – Load bearing panels for dry environment applications
- OSB3 – Load bearing panels for humid environments
- OSB4 – Load bearing panels for heavy-duty applications in humid environments

The International Standard ISO 16864:2009(E) [23] classifies OSB similar to the EN 300, with OSB GP_REG, OSB LB-REG, OSB LB-MR, and OSB HLB-MR representing OSB1, OSB2, OSB3, and OSB4 respectively. While most parts of the world use this standard or an adaptation of this, there are some other classifications for OSB to be found as well. They include the PS 2-18 by the National Institute of Standards and Technology (NIST) in the USA and the CAN/CSA 0325 in Canada [24], [25].

2.4 Thermal Property Tests

2.4.1 Cone Calorimeter Tests

The cone calorimeter test is performed to study the fire behavior of a material. It can be used to determine material properties such as ignition temperature, heat release rate (HRR), mass loss rate, effective heat of combustion, and yields of gas species such as carbon monoxide and carbon dioxide.

White and Winandy (2006) carried out cone calorimeter tests for three 29 mm thick OSB products (referred to as A, B, and C). A and C were of mixed hardwoods and B was southern pine. The ignition time and the peak HRR of the tests can be found in Table 1 [26].

Table 1: Cone calorimeter test results of White and Winandy (2006)
Reproduced from [26]

Product	Radiant heat flux (kW/m ²)	t_{ig} (mean) (s)				HRR_{peak} (mean) (kW/m ²)			
		20	35	50	65	20	35	50	65
OSB A		194.8	38.6	18.7	10.2	168.5	162.9	198.6	252.2
OSB B		305.7	66.3	19.8	13.2	192.6	164.3	191.4	233.7
OSB C		156.6	42.8	16.2	11.1	170.5	181.2	217.8	284.1

Rantuch et al. (2015) performed cone calorimeter tests for OSB3 of thickness 14 mm at five different radiant heat flux values: 20 kW/m², 30 kW/m², 40 kW/m², 50 kW/m², and 60 kW/m². The ignition time and the first peak HRR of the experiments are compiled in Table 2. The theoretical critical heat flux for the material was identified as 16.7 kW/m² [27].

Table 2: Cone calorimeter test results of Rantuch et al. (2015)
Reproduced from [27]

Radiant heat flux (kW/m ²)	t_{ig} (s)	HRR_{peak} (kW/m ²)
20	138	209.3
30	49	195.7
40	24	210.0
50	17	234.0
60	13	301.5

Cone calorimeter tests have also been done by others such as Grexa and Dietenberger [28]–[30]. More recent tests were done by Ira et al. (2020), according to the ISO 5660-1 at three different radiant heat flux values: 20 kW/m², 50 kW/m², and 80 kW/m². The ignition time, time to reach peak HRR, and peak HRR are detailed in Table 3 [31]. The test results of Grexa et al. (1996) and Ira et al. (2020) gave average heat of combustion values of 12.2 MJ/kg and 11.7 MJ/kg respectively.

Table 3: Cone calorimeter test average results of Ira et al. (2020)
Reproduced from [31]

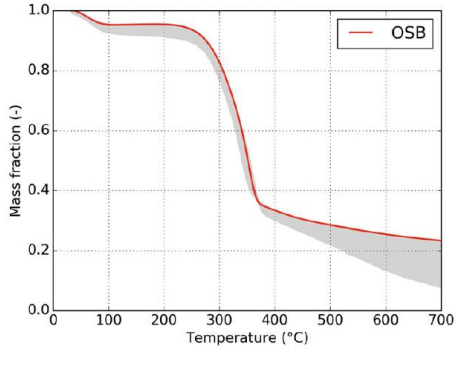
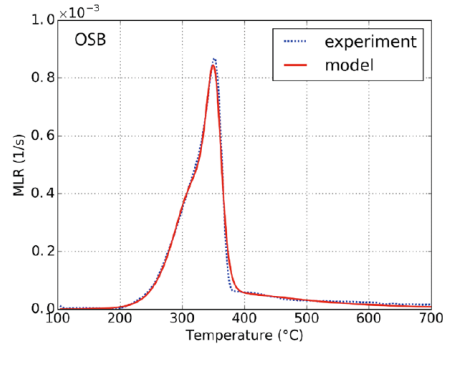
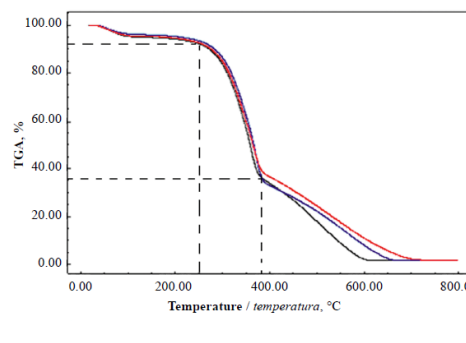
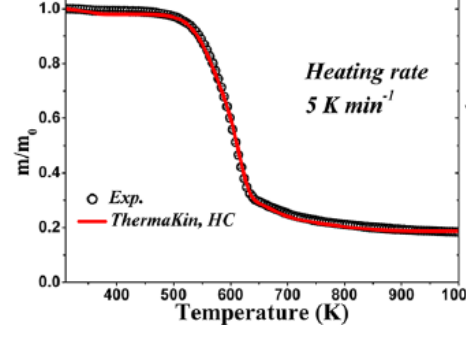
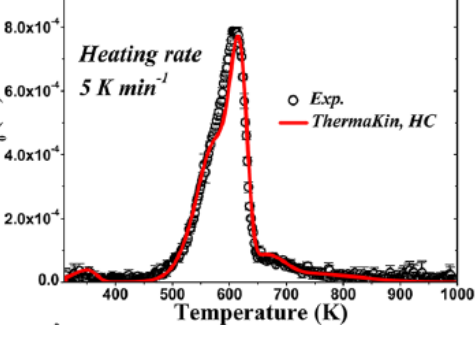
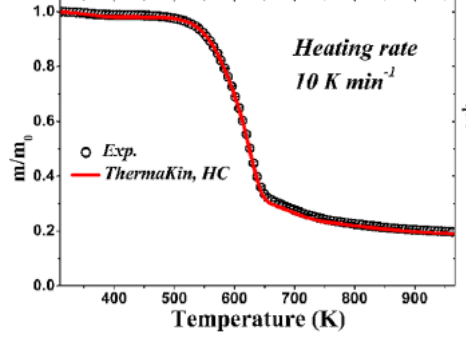
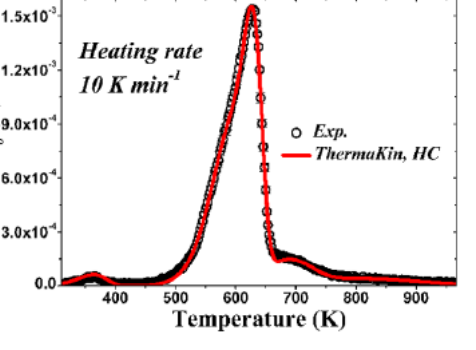
Radiant heat flux (kW/m ²)	t_{ig} (s)	t_{peak} (s)	HRR_{peak} (kW/m ²)
20	188	195	203
50	21	35	250
80	7	16	337

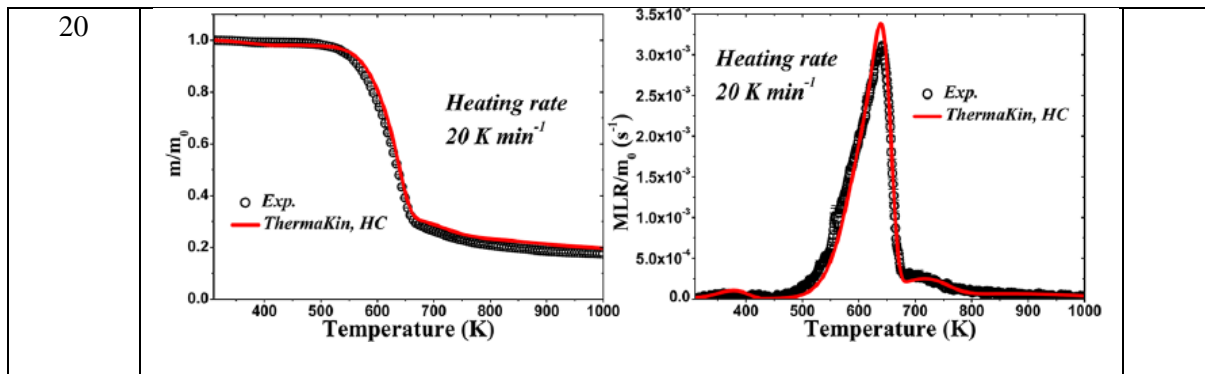
2.4.2 Thermogravimetric Analysis (TGA)

TGA tests are used to measure changes in the mass of a material at a given time and temperature. The results provide quantitative and qualitative information about physical changes in the test sample with response to temperature, heating rate, and atmospheric conditions (inert/oxygen-rich). TGA can be used to quantify material composition, study decomposition, and thermal stability of the material and can also be used as a secondary means of material identification [32].

From literature, it was seen that TGA tests had been performed for OSB by several researchers including Ira et al. (2020), Yapici (2020) (for OSB produced from Scotch pine wood), and Gong et al. (2021). In each case, the tests had been done for ground OSB in a nitrogen atmosphere. The tests were conducted at a heating rate of either 5K/min [31], [33], 10 K/min [6], [33] or 20 K/min [33]. The results of the TGA tests have been compiled in Table 4.

Table 4: Results from past TGA tests

Heating rate (K/min)	Mass fraction as a function of temperature	Derivative thermogravimetric curve	Ref
5			[31] Reproduced with permission from Springer
10			[6] Open access
5			[33] Reproduced with permission from SAGE Publications
10			



From the tabled results above, it can be seen that the results are similar for all three OSB tested. A small mass loss is observed at around 100 °C (between 1% - 8%), which can be attributed to the vaporization of the moisture content in the OSB sample. Other than that, mass loss is minimal until around 250 °C. For the next 100 °C to 150 °C, a large mass loss occurs leaving the remaining mass at around 30% of the initial mass. After this, the mass loss still occurs at an almost steady state, although at a much lower rate. Considering the different heating rates, it is observed that the mass-loss rate (in the major mass loss region) increases with increasing heating rate. This can be seen in the thermogravimetric curves, where the curve shape is similar, and the peak mass loss rate is highest for the 20 K/min heating rate.

Timber is composed of the polymeric material cellulose, hemicellulose, and lignin. These materials are responsible for the strength and rigidity of timber [34]. OSB as a timber product, also consists of the three materials above, with the addition of resin. A suggestion made by Gong et al. (2021) is that the resin content in timber products such as OSB is very small, and so, the thermal decomposition of timber composites must be similar to the thermal decomposition of natural timber [33].

2.4.3 Thermal Conductivity Test

Thermal conductivity is an important parameter when it comes to thermal and heat transfer modelling. Work was done by Sonderegger and Niemz (2009) to measure the thermal conductivity of OSB3 according to ISO 8302. The tests were conducted using the apparatus λ -Meter EP500 (Lambda-Messtechnik GmbH, Dresden). OSB3 samples of thickness 12, 15, 18, 22, and 25 mm and area of 500 mm x 500 mm were conditioned at 20°C and 65% Relative Humidity before testing [35]. The thermal conductivity results at 10 °C were produced as shown by Figure 9.

Thermal conductivity is also dependent on the temperature of the material. For materials such as timber, thermal conductivity linearly increases with increasing temperature [36] for a certain temperature range. Experimental work done by Vololonirina et al. (2014) for OSB in the temperature range 10 °C to 40 °C produced thermal conductivity results that had a linear relationship with temperature as seen by Figure 10. The testing was done for OSB of two different thicknesses (11.3 mm and 20.7 mm). For both thicknesses, the thermal conductivity-temperature relationships were linear, but not equal.

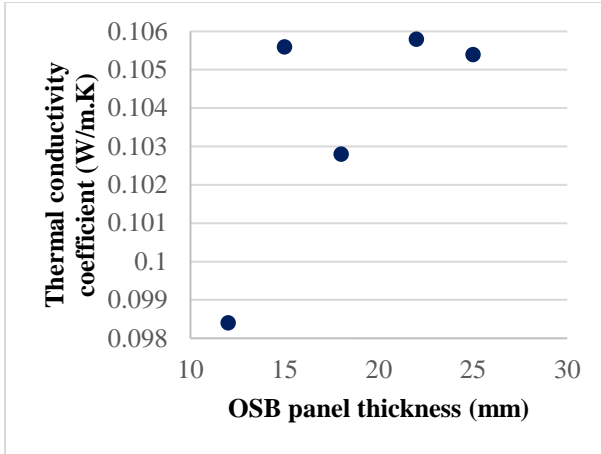


Figure 9: Results of thermal conductivity test by Sonderegger and Niemz (2009)
Produced from [35]

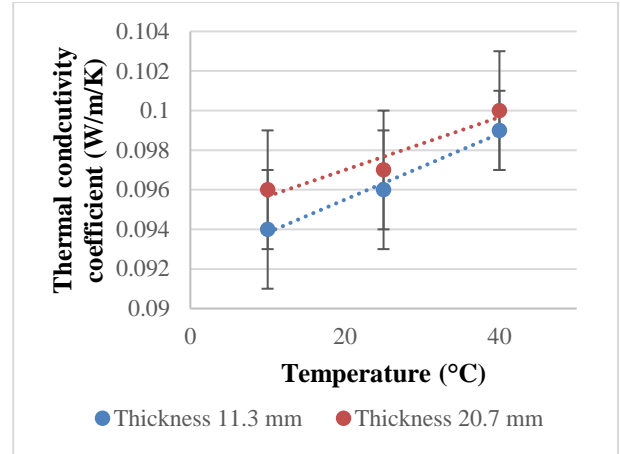


Figure 10: Thermal conductivity of OSB versus temperature by Vololonirina et al. (2014)
Produced from [37]

2.5 Effect of Moisture Content on Thermal Properties of OSB

The moisture content of a material can impact the properties of a material, including thermal properties. As part of the production process of OSB, before the binding the flakes are dried. Therefore, the moisture content of OSB is usually much less than that found in normal timber and is typically in the range of 2% - 8%. Igaz et al. (2017) tested OSB3 board samples varying the moisture content between 0% and 10.14% [38].

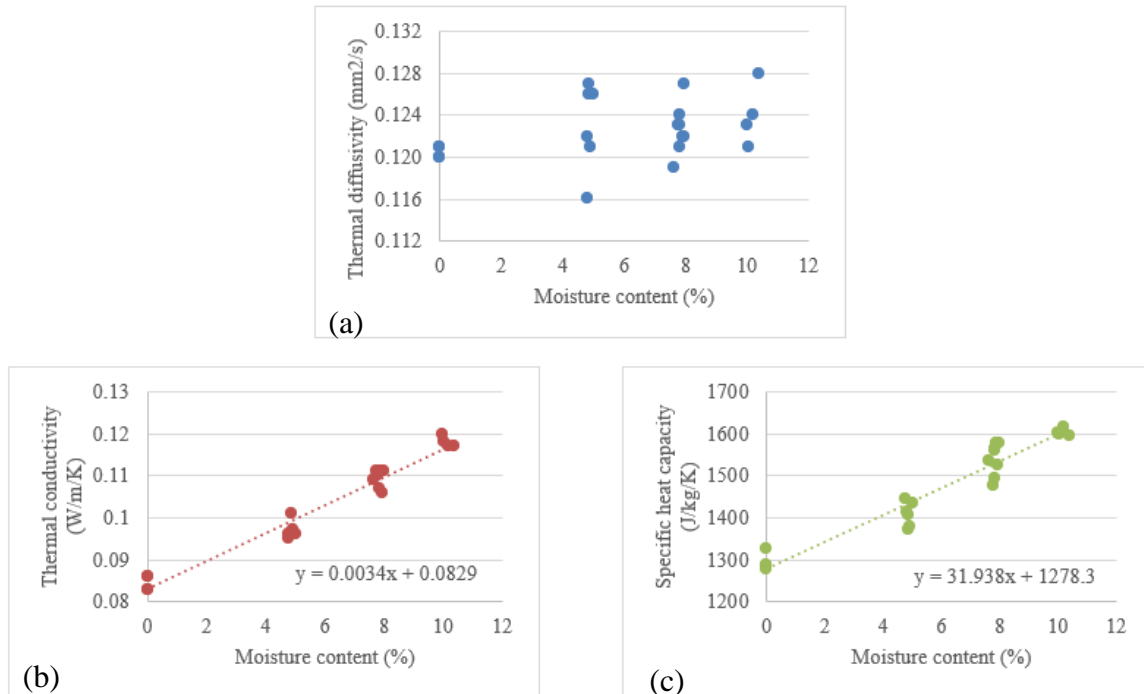


Figure 11: Effect of moisture content on thermal properties of OSB
(a) thermal diffusivity, (b) thermal conductivity, and (c) specific heat capacity. Reproduced from [38]

Prior to the testing, the test specimens were conditioned at 20 °C and 65% relative humidity for 14 days and oven-dried at 103 °C to remove all moisture. Afterwards, the thermal diffusivity, thermal conductivity and specific heat capacity of the specimens were tested at an ambient temperature of 21 ± 1 °C.

Moisture content of OSB can directly affect thermal properties such as thermal diffusivity, thermal conductivity and specific heat capacity as shown by the experimental results of Igaz et al (2017) (Figure 11). For both thermal conductivity and specific heat capacity, the properties increase linearly with an increase in moisture content.

2.6 Mechanical Performance of OSB

By looking at the manufacturing process of OSB, it is clear that the material is not homogeneous. This means the cut of the specimen will dictate its mechanical strength.

Compression and tensile tests were done for OSB by Chen and He (2017) according to the BS EN 789 (2005) standards [39]. Samples were taken angled 0°, 45°, and 90° to the OSB panel (Figure 12) and named s, x, and h respectively. The specimens for compression were made by taking five samples of 9.5 mm x 50 mm x 240 mm and bonding them together using outdoor epoxy adhesive. Similarly, the tensile specimens were made by bonding five samples of dimension 9.5 mm x 90 mm x 400 mm. A visual of the tensile and compression specimens is shown in Figure 13.

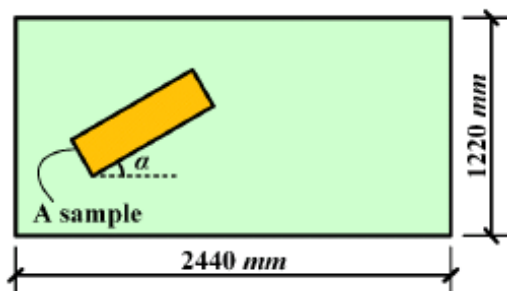


Figure 12: Cutting patterns of specimens
Reproduced from [39] (Open access)

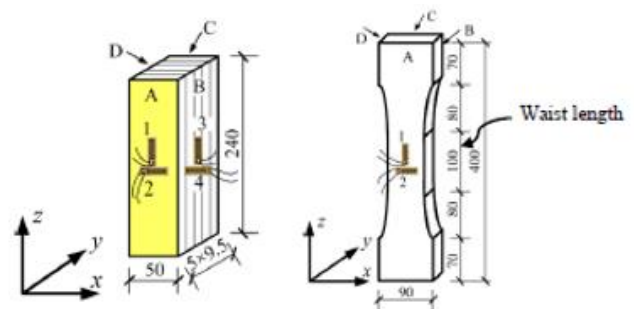


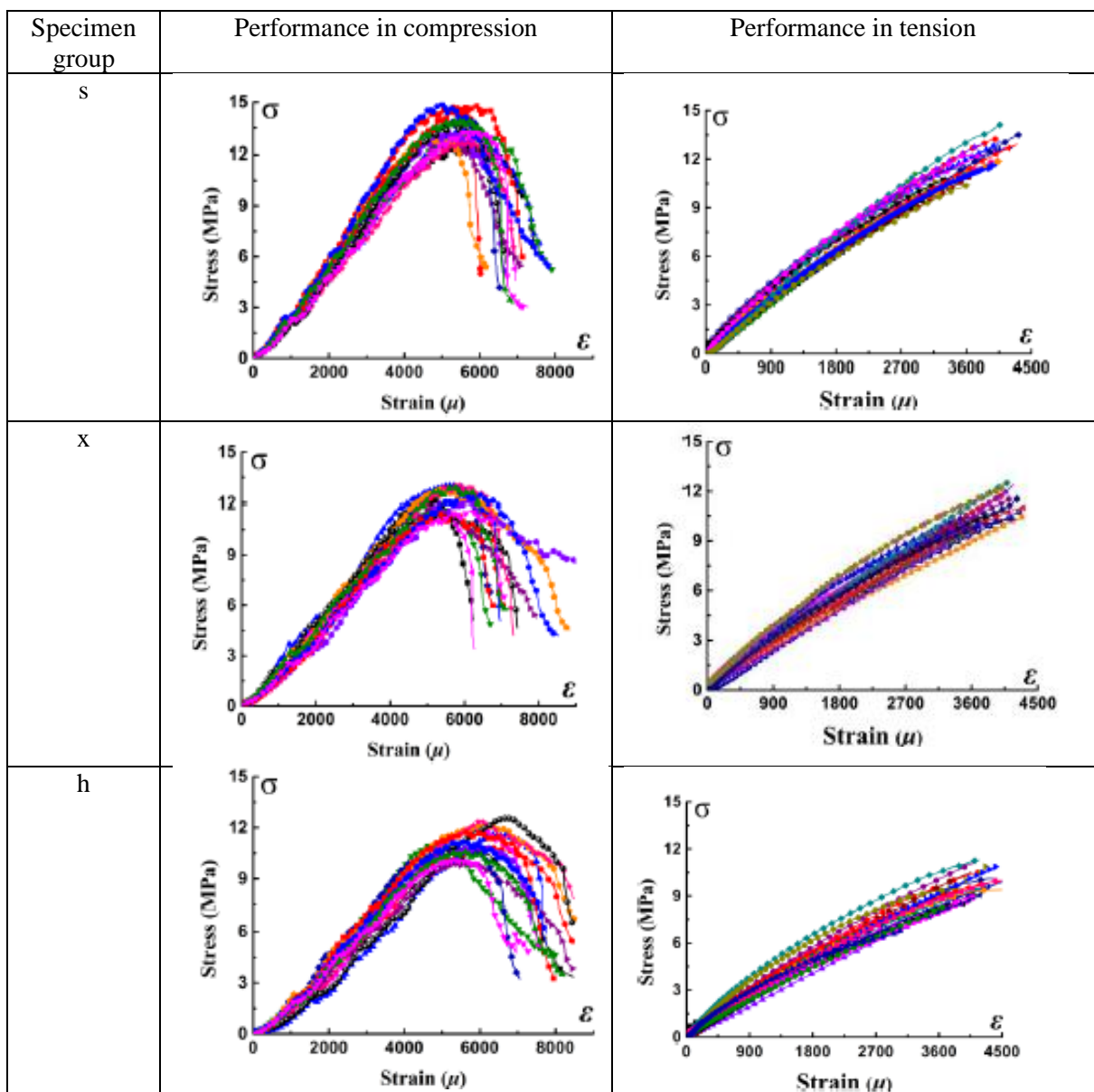
Figure 13: Specimens for compression and tensile tests respectively
Reproduced from [39] (Open access)

Table 6 gives the stress-strain relationship for the tests. For the compression loading, a linear behavior can be observed up to around 60% of maximum stress. For the tensile loading, linear behavior was seen until failure. As can be seen from the graphs, there was a significant difference for both compression and tension tests with the different angles when cutting specimens. The maximum carrying capacity, compressive/tensile strength, and modulus of elasticity of the compression and tensile tests are summarized in Table 5.

Table 5: Summarization of compression and tensile tests of Chen and He (2017)
 Reproduced from [39]

Specimen group	Compression tests			Tension tests		
	Max. carrying capacity (kN)	Compressive strength (MPa)	Modulus of elasticity (MPa)	Max. carrying capacity (kN)	Tensile strength (MPa)	Modulus of elasticity (MPa)
s (0°)	32.74	13.6	3253	6.96	12.1	3155
x (45°)	30.54	12.5	2769	6.32	10.9	2762
h (90°)	27.57	11.3	2487	5.81	9.7	2326

Table 6: Stress-strain graphs for the experimental results of Chen and He (2017)
 Reproduced from [39] (Open Access)



2.7 Experiments Linking Mechanical Strength of OSB with Thermal Conditions

Evidence shows that deterioration of wood is minimal at an exposure temperature of 100 °C [40]. However, considering that OSB is a composite containing resin as adhesive, it could experience deterioration at 100 °C which could cause a loss of strength. In this section, previous experiments investigating the loss of strength of OSB with elevated temperatures have with reviewed.

Sinha et al. (2011) carried out 576 four-point bending tests (as shown in Figure 14) for 576 specimens of OSB (aspen) in the dimension of 406 mm x 76 mm x 11.12 mm [10]. The tests were divided into 72 exposure time-temperature groups with 9 different temperatures (50,75, 100,125, 150, 175, 183, 191, and 200 °C) and 8 exposure times (ranging from 1 hour to 8 hours at 1-hour increments).

After being exposed to the high temperature, each specimen was left to cool down at room temperature for 24 hours before the four-point bending test was performed. The span used was 304.8 mm and the loading rate was 8 mm/min.

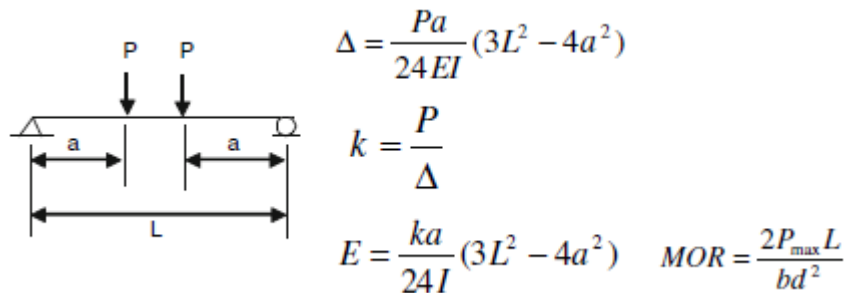


Figure 14: Four-point bending test ($a = L/3$)

Figure 15 described the influence of temperature on the bending strength of OSB. As can be seen, not only the temperature, but the exposure time also affects the bending strength.

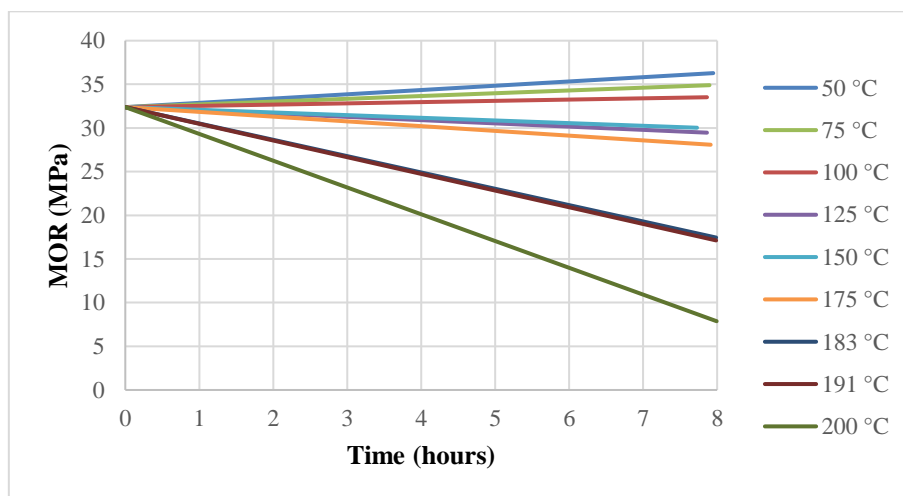


Figure 15: Summary of the bending tests for OSB by Sinha et al. (2011)
Reproduced from [10] with the permission of Springer Nature

The work done in the paper concluded that OSB has a degradation rate $k(T) = 2E6 e^{-6510/T}$ and the apparent activation energy is 54.1 kJ/mol.

Bekhta et al., (2003) conducted a bending test for OSB specimens of 300 mm x 50 mm x 22 mm at temperatures of 20, 40, 60, 80, 110, and 140 °C [41]. Five specimens were used for each temperature. Before heating, the specimens were conditioned at 20 °C and 65% relative humidity for two weeks. The specimens were subject to a constant high temperature for one hour, then mechanically tested. The test results have been detailed in Figure 16 and Table 7.

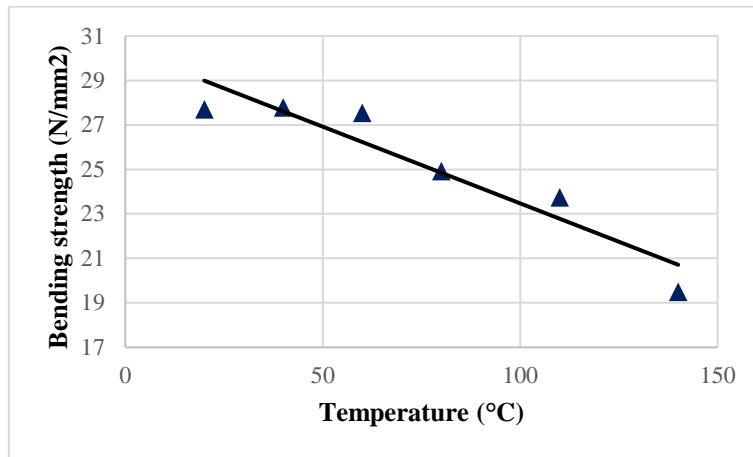


Figure 16: Summary of thermal-mechanical tests for OSB by Bekhta et al. (2003)
Reproduced from [41] with permission from Springer Nature

Table 7: Reduction of mass and bending strength of OSB at different temperature levels
Reproduced from [41] with permission from Springer Nature

Temperature of heat treatment (°C)	Reduction of bending strength (%)	Weight loss (%)
40	0.4	0.79
60	1.4	1.56
80	10.7	2.91
110	15	4.94
140	30	7.12

3 Experimental Methodology

To increase the understanding of the thermal behavior of OSB, a set of thermal material property tests and thermal-mechanical combination tests were executed. These test results will be compared against results found in the literature study. This section describes each of the experimental procedures including the specimen preparation, apparatuses, and the testing process.

3.1 Specimen Specifications

The specimens used for the testing in this project were sourced from an OSB3 (unsanded) board produced by the company KRONOSPAN Riga. The intended use of the material is for internal use as a structural component in humid conditions.

The factory number for the material is OSB3-CPR-2013-07-01-8.

The thickness of the used board was given as 11.0 mm.

The detailed declaration of the performance of the material given by the production company has been attached in Appendix 11.1.

3.2 Thermal Property Tests

3.2.1 Thermal Conductivity Test

The test was conducted using the Netzsch Heat Flow Meter apparatus. A sample of 300 mm x 296 mm and 10.5 mm thickness was used. The mass of the sample was 532.87 g, and the density was calculated to be 571.5 kg/m³. The sample was tested between the temperature of 15°C and 85°C. Considering that the surface of the OSB3 is not perfectly even, insulation mats were used below and above the sample.

In the apparatus, the OSB3 specimen was placed between a hot plate and cold plate at controlled temperatures and temperature gradient ($\Delta T/t$). The specimen thickness (t) was measured using an internal gauge. During the testing period, the heat flow through the specimen (\dot{Q}) was measured using two calibrated heat flux transducers. The testing was concluded upon reaching thermal equilibrium [42].

3.2.2 TGA Test

The test was conducted using the Netzsch Simultaneous Thermal Analyzer – STA 449 F3 Jupiter® apparatus. The test sample was prepared by grinding the OSB3 into a powder. The sample was heated at a constant rate from 30 °C to 400 °C. The air conditions used were 100% N₂ atmosphere.

Specimen samples were taken from three locations of the OSB3 panel. For each location specimen, TGA tests were conducted at three heating rates: 5 K/min, 10 K/min, and 20 K/min. Overall, nine TGA tests were performed. Each test was done without a prior drying cycle.

3.2.3 Cone Calorimeter Test

The cone calorimeter tests were conducted using the guidelines given in ASTM E1354 and ISO 5660 [43], [44]. The apparatus can be seen as shown in Figure 17. The test samples were prepared in dimensions of area 100 mm x 100 mm. The thickness of the OSB3 samples was measured to be between 10.6 mm and 11.0 mm. Prior to the testing, the samples were kept in a conditioning chamber under the conditions of 23 °C and 50% relative humidity for approximately 72 hours.



Figure 17: Set-up of the cone-calorimeter apparatus

For each test, two OSB3 specimens, one on top of the other, were used. Thermocouples were attached to the bottom, between the 2 samples and on the surface. Each specimen set was wrapped in foil on the four sides and bottom. This was to prevent the pyrolysis gases from moving from the sides and keep the problem one dimensional. The material was placed in the sample holder and the unexposed side was further covered by an insulation material (ceramic wool). This setup of the materials is described by Figure 18.

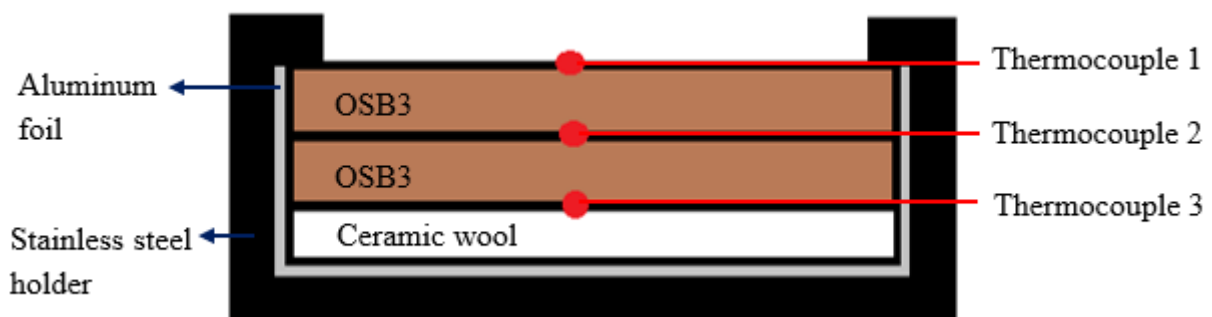


Figure 18: Setup of the OSB3 material with the thermocouples in the cone calorimeter test

After the initial set-up of the apparatus, the temperature of the heating coils was adjusted so that the radiant heat flux would reach the required value and remain steady within a range of 1% of that value. When the required heat flux was reached, the recording of data was started, and after a minimum of 60 s, the sample in the sample holder was introduced into the cone calorimeter. The ignition delay time was recorded, as well as other data of the gases collected

by the exhaust hood. Overall, seven separate tests were conducted, at radiant heat flux values of 35 kW/m², 25 kW/m², and 15 kW/m².

3.3 Thermal-Mechanical Test

This section discusses the experimental work performed to observe the short-term and long-term effects of different thermal conditions on the mechanical strength of OSB3. The results were used to calculate failure stress and strain values of OSB3 and compared against previous work found in the literature.

3.3.1 Equipment

The main two pieces of equipment used were the furnace (Figure 19) and the three-point bending test rig (Figure 20). The loading on the bending test rig was done mechanically using a high-pressure pump. The loading rate was controlled using a foot pedal. The rig was also connected to a load cell (capacity 3000 N) and displacement transducer (capacity 50 mm) at the loading point, allowing loading force and displacement to be measured.



Figure 19: Furnace used to heat OSB3 samples

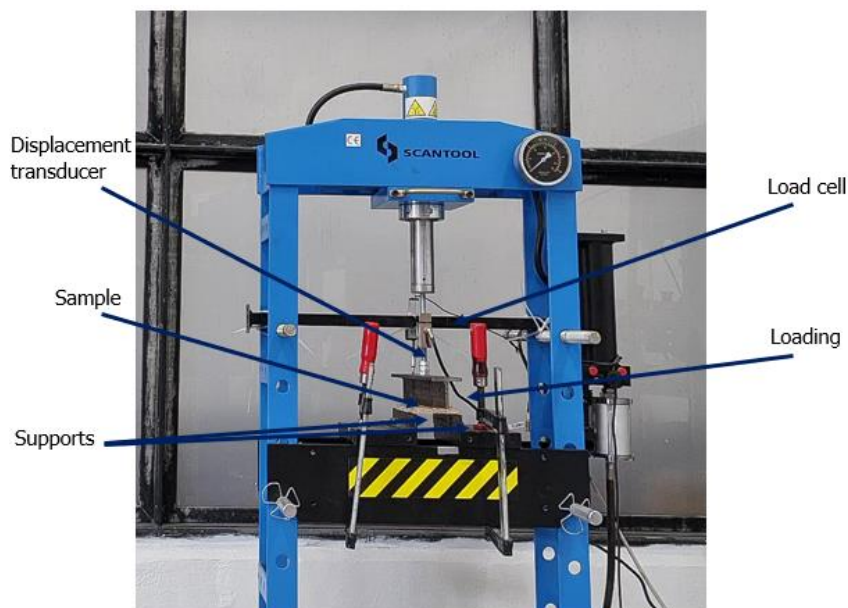


Figure 20: Three-point bending test rig

3.3.2 Specimen Preparation

For this test, sample specimens were prepared in the dimensions of 120 mm x 100 mm. Prior to commencing the tests, the specimens were stored in a conditioning room at a temperature of 23 ± 2 °C and relative humidity of $50 \pm 5\%$ for a minimum of 48 hours.

3.3.3 Heating OSB Samples

The tests were performed for OSB3 subjected to six different temperatures: 50 °C, 75 °C, 100 °C, 150 °C, 175 °C, and 200 °C. The furnace was heated to the required temperature. Once the furnace reached the required steady-state temperature, the OSB3 sample, as well as another similar OSB3 sample with a thermocouple attached to the center (as seen in Figure 21), were placed inside. The temperature increase in the center of the OSB3 was monitored. Once the center of the OSB3 sample reached the furnace temperature, the timer was started for one hour. For each temperature level, 8 – 10 specimen samples were used.



Figure 21: Attaching thermocouple to the center of OSB3 sample

3.3.4 Three-Point Bending Test

For the specimen samples heated at each temperature level, half of the specimens were kept in a conditioning room to cool down for 24 hours before testing. The other specimens were tested as they were taken out of the furnace.

For the bending test, each OSB3 specimen was placed in the three-point bending test rig and subjected to mechanical loading. The span length was kept at 86 mm. For each test, the longitudinal direction of the OSB3 sample was kept parallel to the loading bar.

In addition to the heated samples, 5 specimens kept at room temperature were also tested.

4 Experimental Results

This section describes the results of each of the tests detailed in section 1. In sub-section 4.1, the results of the thermal material property tests (thermal conductivity test, TGA tests, cone calorimeter tests) are discussed. In the next sub-section 4.2, the results of the thermal-mechanical combination tests are discussed.

4.1 Thermal Property Tests

This subsection describes the results of the thermal conductivity test, TGA test and cone calorimeter tests performed on OSB3.

4.1.1 Thermal Conductivity Test

The thermal conductivity test measured the temperatures of the hot and cold plate in the apparatus as well as the heat flow through the specimen for the mean specimen temperatures in the range of 15.2 °C and 84.1 °C. The results were used to calculate the thermal resistance (t/k), temperature gradient, and thermal conductivity coefficient. The thermal conductivity coefficient (k) values have been calculated using equation (1).

$$k = \frac{\dot{Q}t}{A\Delta T} \quad (1)$$

These results are shown in Table 8.

Table 8: Thermal conductivity test readings

Mean temperature (°C)	Thermal difference (K)	Thermal conductivity coefficient (W/(m·K))	Thermal resistance ((m ² ·K)/W)	Temperature gradient (K/m)
15.2	8.3	0.09481	0.1108	787.37
20.1	16.4	0.09707	0.1082	1563.04
29.9	16.4	0.09930	0.1057	1559.75
39.8	16.3	0.10116	0.1038	1555.02
49.6	16.3	0.10350	0.1015	1552.93
59.5	16.3	0.10612	0.0989	1549.63
69.3	16.2	0.10931	0.0961	1544.74
79.1	16.3	0.11208	0.0937	1551.87
84.1	8.3	0.11082	0.0948	787.64

The variation of the calculated thermal conductivity with the change in mean temperature in the specimen has been graphed as shown in Figure 22.

The thermal conductivity coefficient has increased from 0.095 W/m/K to 0.111 W/m/K with the temperature increase from 15.2 °C to 84.1 °C. The average thermal conductivity for the material is 0.1 W/m/K. At the temperature range for which the test was conducted, the chart shows that the thermal conductivity coefficient variation is linear. The relationship between the thermal conductivity coefficient of OSB3 and the average temperature in Celsius and Kelvin respectively can be given by equations (2) and (3).

$$k = 2.44 \times 10^{-4} \times T(^{\circ}\text{C}) + 0.09168 \quad (2)$$

$$k = 2.44 \times 10^{-4} \times T(\text{K}) + 0.02500 \quad (3)$$

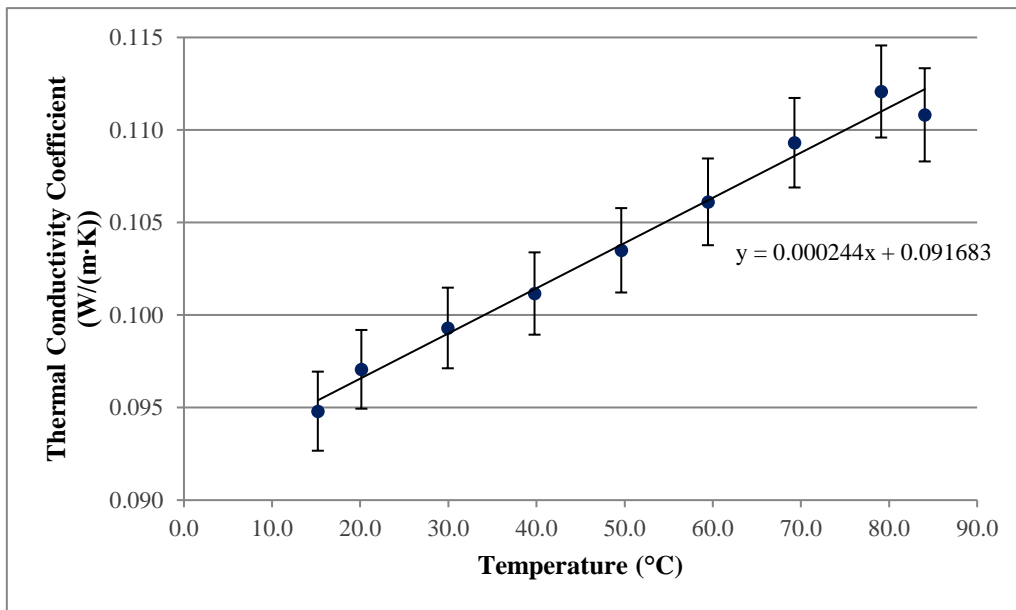


Figure 22: Variation in thermal conductivity coefficient with temperature

4.1.2 TGA Test

4.1.2.1 Mass loss and mass loss rate

The TGA tests were conducted at the heating rates of 5 K/min, 10 K/min, and 20 K/min and in a complete nitrogen environment. The tests measured and recorded sample mass and temperature at periodic time intervals. From the recorded data, for each test, the mass loss rate at each temperature level was also calculated. The graphs of mass versus temperature and mass loss rate versus temperature are displayed in Figure 23 and Figure 24 respectively. For each heating rate, three TGA tests were performed. The results shown by the graphs give one graph line for each heating rate by combining the results of all three TGA performed for each heating rate. The combining was done by averaging the three individual curves.

As observed in Figure 23, the mass loss is minimal until around 225 °C, at which point the mass loss is around 1.8% - 2.0%. The mass loss with temperature is significant from that point until the sample mass reaches around 32%. This point is reached at the lowest temperature of 370 °C for the tests at a heating rate of 5 K/min. For the tests at the heating rates of 10 K/min and 20 K/min, this point is reached at the temperatures of 380 °C and 390 °C respectively. Upon reaching the previously mentioned mass percentage, the mass-loss rate is reduced again until the final test temperature of 400 °C. The mass percentage recorded at the final test temperature is in the range of 30.9% - 31.7%.

In the temperature range that the major mass loss occurred, the mass-loss rate varies in a similar pattern for each heating rate. For each mass loss rate curve, a peak is observed. This peak is observed to be largest for the largest heating rate of 20 K/min and lowest for the lowest heating

rate of 5 K/min. The temperature corresponding to the peak of the mass-loss rate also increased with increasing heating rate.

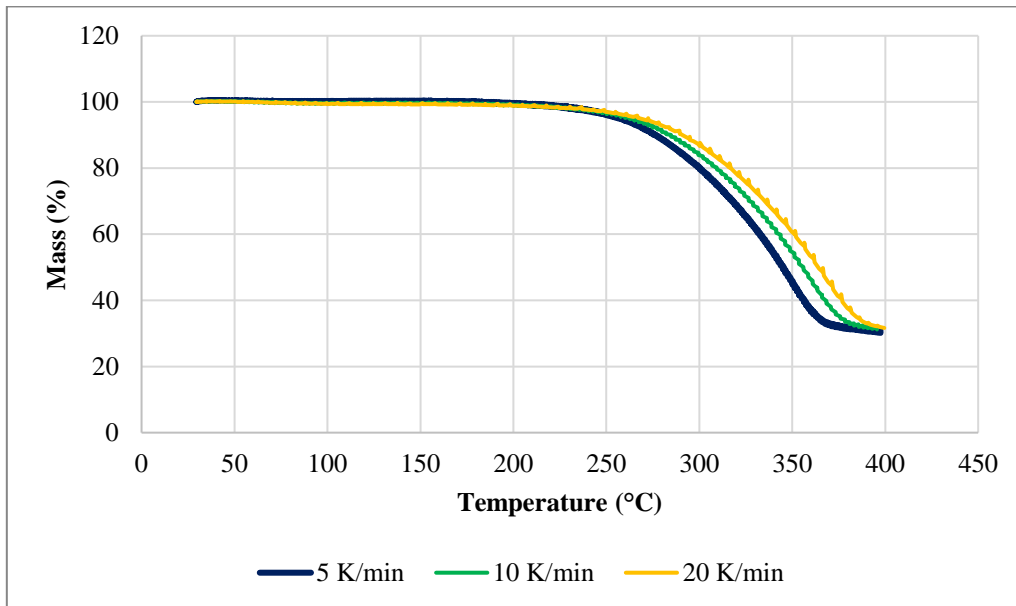


Figure 23: Variation of mass with temperature in TGA test

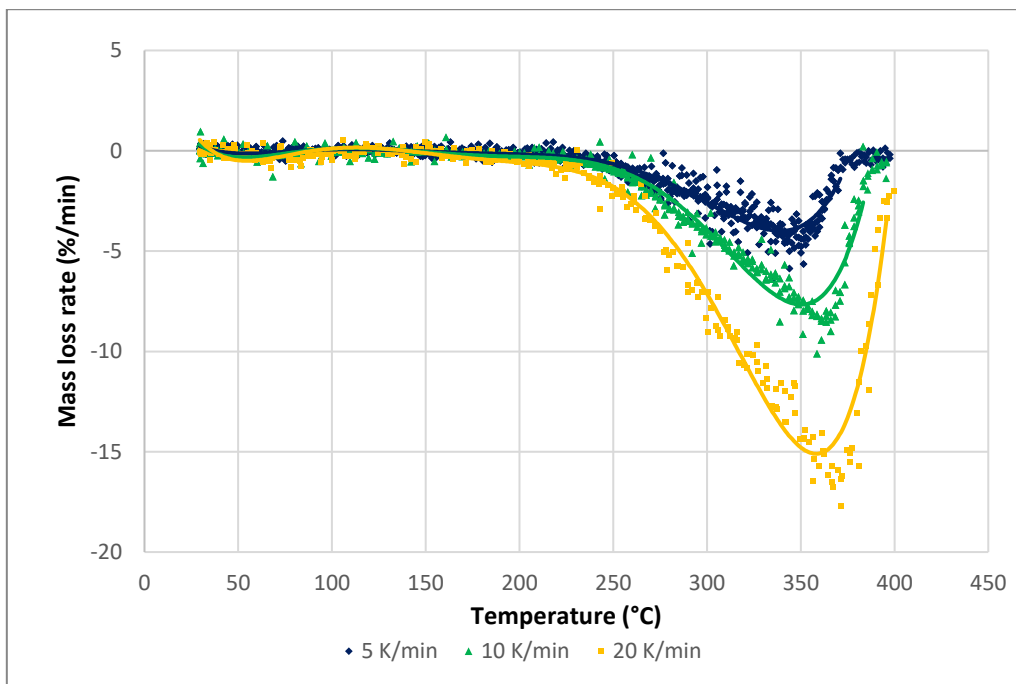


Figure 24: Variation of mass loss rate with temperature in TGA tests

4.1.2.2 Moisture content

The results of the nine TGA tests were used to calculate the moisture content in the material. The mass losses at 95 °C, 100 °C, 105 °C, and 110 °C were calculated as given by Table 9. At these temperature points, it was assumed that the mass loss was only due to the loss of moisture. Considering the sample was in ground form during the testing, it was assumed that by 110 °C, all of the moisture present in the test samples had been evaporated.

Table 9: Calculated mass loss (%) from TGA results

Test Number	Heating rate (K/min)	Temperature			
		95 °C	100 °C	105 °C	110 °C
1	5	0.29%	0.26%	0.23%	0.24%
2		0.49%	0.48%	0.45%	0.48%
3		0.25%	0.22%	0.23%	0.21%
4	10	0.69%	0.74%	0.72%	0.75%
5		0.72%	0.73%	0.73%	0.73%
6		0.49%	0.55%	0.53%	0.49%
7	20	0.76%	0.81%	0.82%	0.89%
8		0.51%	0.62%	0.48%	0.59%
9		0.71%	0.75%	0.76%	0.80%
Average		0.55%	0.57%	0.55%	0.58%
Minimum		0.25%	0.22%	0.23%	0.21%
Maximum		0.76%	0.81%	0.82%	0.89%

For the nine test samples, the moisture content was found to range between 0.21% and 0.89%. The lowest average was calculated to be 0.55% at 105 °C. These calculated values are much lower than the typical range of moisture content for OSB3. The moisture content of the OSB3 could also be investigated using another method in future studies to assess the accuracy of the current calculations.

4.1.3 Cone Calorimeter Test

Overall, seven cone calorimeter tests were conducted at radiant heat fluxes of 15 kW/m², 25 kW/m², and 35 kW/m². Figure 25 provides some visuals of the OSB3 sample during the cone calorimeter tests and afterwards.



Figure 25: OSB3 sample during cone calorimeter test and afterwards

During the flaming, the OSB3 material was observed to expand, as can be seen from the images above. This phenomenon was reduced when using the metal wireframe on the sample surface. Since each test used two stacked OSB3 pieces, there is the possibility that the material expansion can cause a separation between the two pieces. Therefore, when expansion occurs it can't be assumed that heat transfer from the surface to the bottom of the test sample occurs only through heat conduction.

4.1.3.1 Temperature measurements

The temperature measurements were taken at the center of the surface, middle and bottom of the OSB3 samples. The temperature versus time was plotted for the recordings for the tests conducted at each radiant heat flux as shown by Figure 26, Figure 27, and Figure 28. For each figure, graph (a) displays the complete plot, with the red line denoting the point of ignition. Graph (b) described the plot from the start of the test until the point of ignition.

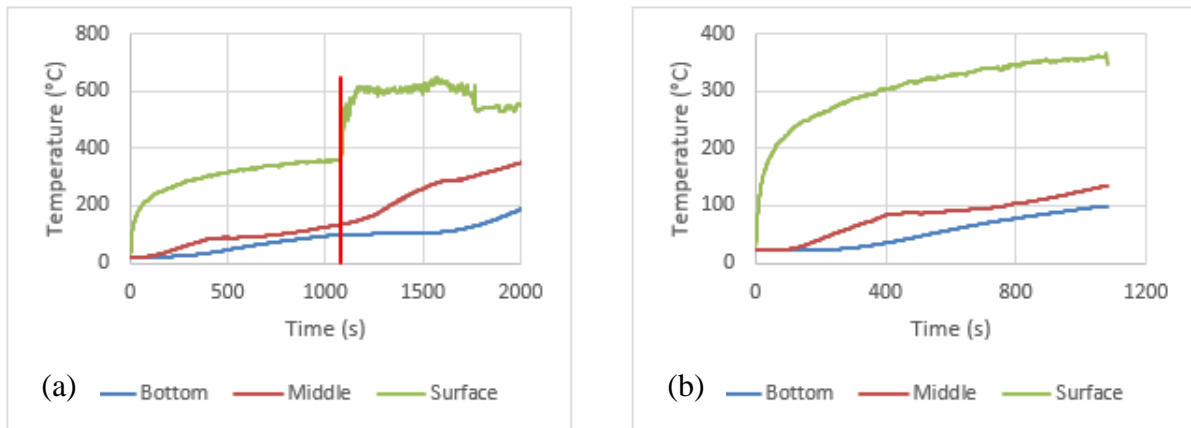


Figure 26: Temperature reading for cone calorimeter test (15 kW/m^2)
 a) Entire duration of the test, b) From start until the ignition point

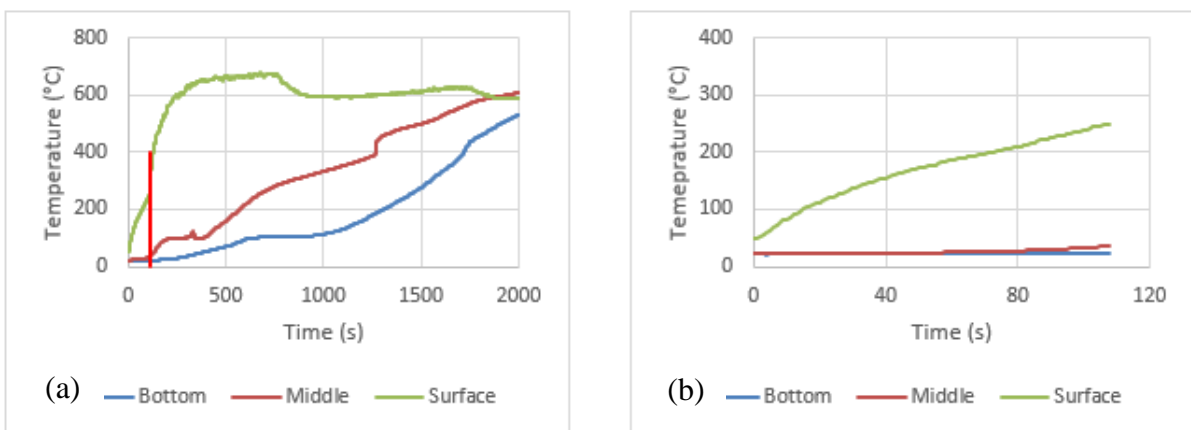


Figure 27: Temperature reading for cone calorimeter test (25 kW/m^2)
 a) Entire duration of the test, b) From start until the ignition point

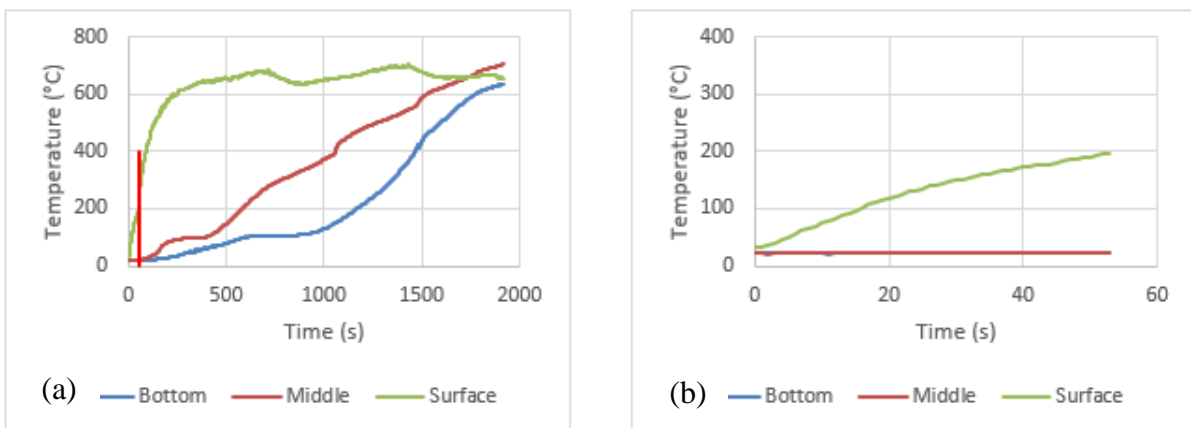


Figure 28: Temperature reading for cone calorimeter test (35 kW/m^2)
 a) Entire duration of the test, b) From start until the ignition point

According to the temperature readings of the thermocouples, the temperatures of the OSB3 samples at which piloted ignition occurred were identified. These ignition temperature values are compiled in Table 10. It is clearly observed that the measured ignition temperature changes with the radiant heat flux value, with higher ignition temperatures observed for the lower radiant heat fluxes.

Table 10: Ignition temperature for each cone calorimeter test

Test number	\dot{Q}_R'' (kW/m ²)	T_{ig} (°C)
1	15	348
2	15	321
3	25	196
4	25	192
5	25	250
6	35	198
7	35	150

4.1.3.2 Critical heat flux

The critical heat flux (CHF) is a theoretical value that can be defined as the lowest radiant heat flux at which autoignition will occur. Mathematically, for CHF, $t_{ig} \rightarrow \infty$, meaning, $1/t_{ig} \rightarrow 0$. The inverse of ignition time was plotted against the radiant heat flux [45] as given by Figure 29. Based on the plotted data, the CHF for the material was calculated to be 14.6 kW/m².

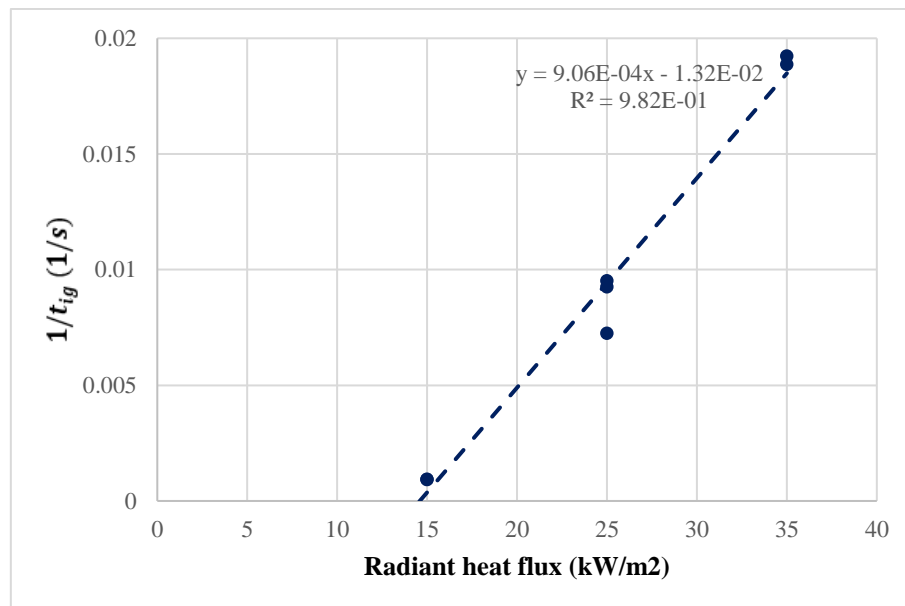


Figure 29: Graph of $1/t_{ig}$ vs radiant heat flux in cone calorimeter test

4.1.3.3 Heat release rate

The heat release rate curves were plotted for each of the cone calorimeter tests performed, as displayed in Figure 30.

The average effective heat of combustion was also calculated for the material, for each HRR curve, using equation (4).

$$\Delta h_{c,eff} = \frac{\sum_i \dot{q}_i \Delta t}{m_i - m_f} \quad (4)$$

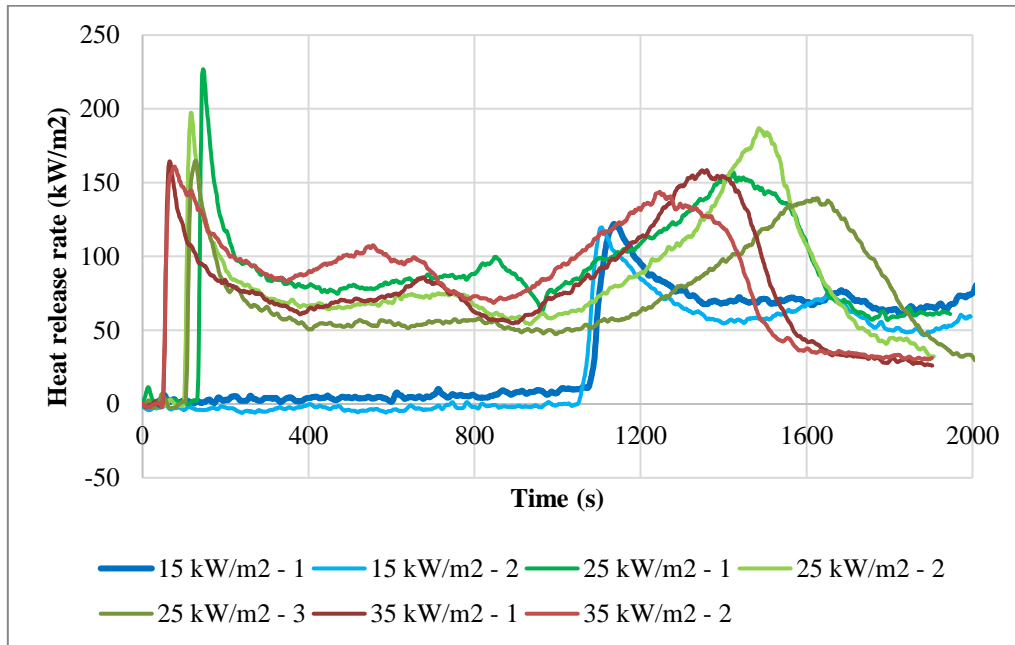


Figure 30: Heat release rate curves of the cone calorimeter tests

Table 11 gives a compilation of the first peak HRR, the time to reach that peak and the average effective heat of combustion for each cone calorimeter test. The highest peak HRR was observed for a test conducted at a radiant heat flux of 25 kW/m², at 227 kW/m². The lowest peak HRR was observed for the tests conducted at a radiant heat flux of 15 kW/m² at 120 kW/m². The calculated average effective heat of combustion is in the range of 1026 kJ/kg – 1621 kJ/kg.

Table 11: Peak HRR, time to reach peak HRR and average effective heat of combustion

Test number	\dot{Q}_R'' (kW/m ²)	t_{ig} (s)	t_{peak} (s)	HRR_{peak} (kW/m ²)	$\Delta h_{c,eff}$ (kJ/kg)
1	15	1080	1134	122	1341
2	15	1062	1104	120	1026
3	25	138	146	227	1621
4	25	105	115	197	1459
5	25	108	126	165	1433
6	35	53	63	164	1469
7	35	52	75	161	1523

4.2 Thermal-Mechanical Tests

This sub-section describes the results of the thermal-mechanical combination tests performed on OSB3. Initially, the temperature measurements done in the center of the test specimens inside the furnace will be discussed, followed by the results of the three-point bending tests performed.

4.2.1 Temperature Measurements

Prior to the bending test, the OSB3 specimen samples were placed in the furnace which was kept in a steady temperature state. The center of an additional OSB3 sample was measured and recorded. The temperature variation with time is plotted in Figure 31. The time at which the specimen center reached the temperature of the furnace (steady-state) was also observed and recorded. This time is denoted on the graph by the black vertical lines on each curve. Figure 32 gives a plot of the time taken to reach the furnace temperature in the sample center against the testing temperature.

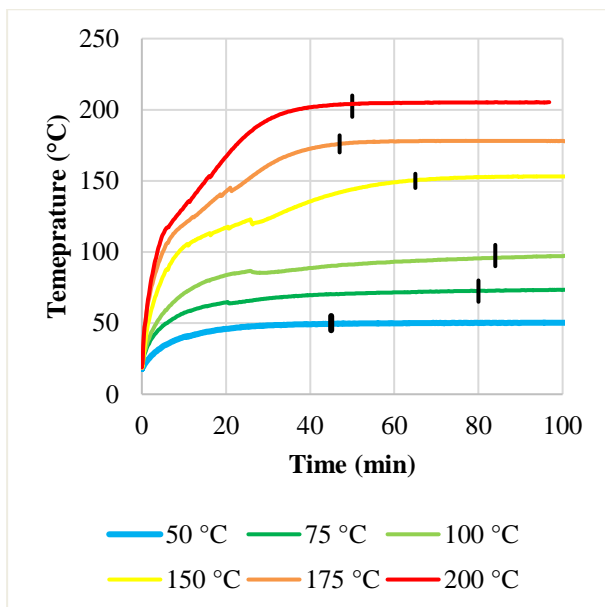


Figure 31: Variation of temperature with time in OSB3 specimen center in the furnace

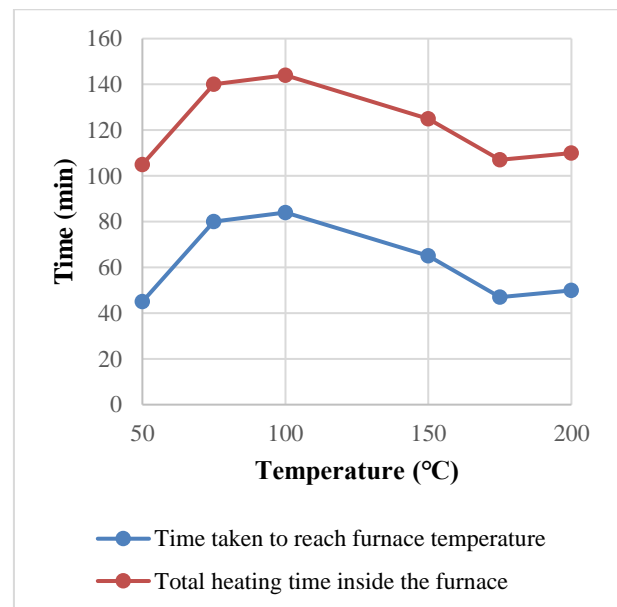


Figure 32: Time OSB3 samples were kept in furnace in the thermal-mechanical tests

As seen by the figures above, the temperature -time curves behave similarly for each testing temperature. However, the time taken for the specimen center to reach the testing temperature is not similar. Considering the different testing temperatures, this time was less than one hour for the testing temperatures of 50 °C, 175 °C, and 200 °C and the time was more than one hour for 75 °C, 100 °C, and 150 °C.

4.2.2 Visual Analysis and Mass Loss of Thermal Condition Impact

Any visual changes occurring on the material surface after removal of the specimens from the furnace were observed. Figure 33 displays the OSB3 specimens at room temperature and upon being exposed to different thermal conditions in the furnace.

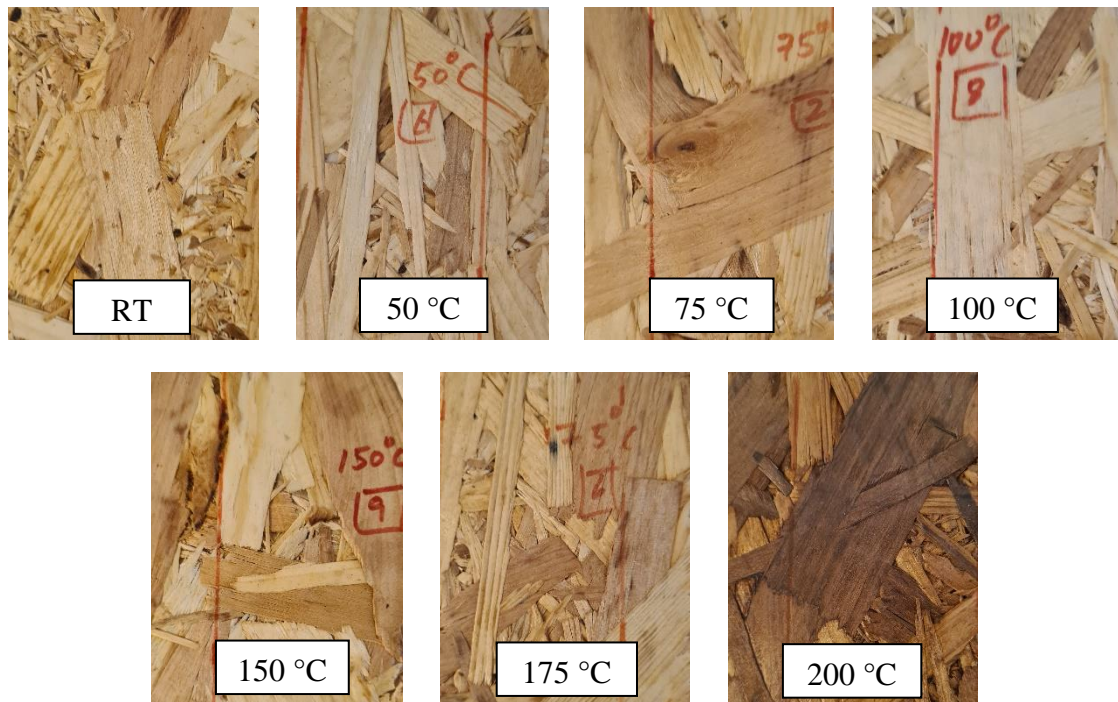


Figure 33: Visual of test samples upon removing from the furnace

For the specimens exposed to temperatures of 50 °C, 75 °C, and 100 °C, no visual change was observed in the surface timber strands. For the 150 °C temperature exposed specimens, a slight darkening of the timber stands on the surface was observed. A similar shade of darkening was seen in the specimens exposed to 175 °C. However, for the specimens exposed to 200 °C, a significant change in color was observed, including the initial charring of the timber strands.

From mass measurements of specimens before placing them in the furnace and after removing them, the average mass loss was calculated for each test temperature as shown in Table 12. From 100 °C to 175 °C, the mass loss difference was minimal, with the mass loss ranging from 5.14% to 5.46%. The mass loss at 100 °C was 5.2%, and if the contribution to the mass loss at 100 °C is assumed to be solely from the moisture present, it can be considered that the moisture content is also equivalent to around 5.2%.

Table 12: Average mass loss at each temperature level

Temperature	50 °C	75 °C	100 °C	150 °C	175 °C	200 °C
Mass loss	1.40%	3.02%	5.20%	5.14%	5.46%	9.37%

4.2.3 Three-Point Bending Test

After subjecting the OSB3 specimens to different steady thermal conditions, the specimens were subjected to a three-point bending test. During the testing, the subjected load and displacement of the testing sample at the loading line were recorded against time. From the data collected, the flexural stress and strain were calculated using equations (5) and (6) for each test.

$$\sigma_b = \frac{3PL}{2bd^2} \quad (5)$$

$$\varepsilon_b = \frac{6Dd}{L^2} \quad (6)$$

From the performed calculations, the stress-strain curves were plotted for each test specimen. Figure 34 and Figure 35 were plotted so that there is a stress-strain curve from each test temperature. For each test temperature, the stress-strain curve was selected so that the failure load closely represents the average failure load for that test temperature. Figure 34 represents the bending tests that were performed for OSB3 specimens upon immediately removing from the furnace. Figure 35 represents the bending tests that were performed for OSB3 specimens after leaving them for a cooling period of 24 hours upon removal from the furnace.

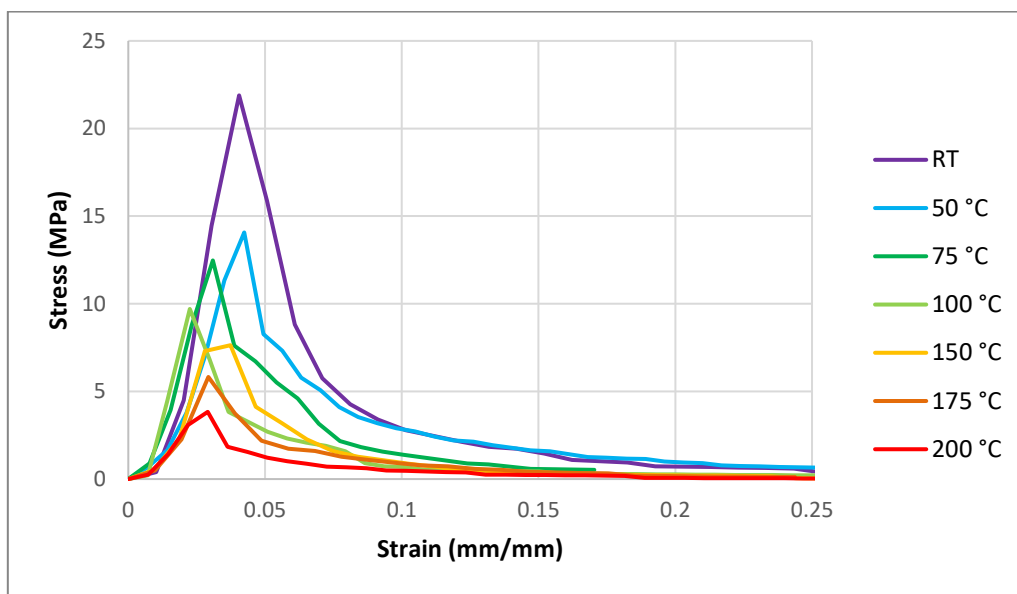


Figure 34: Stress-strain graph – Mechanical testing immediately after heating

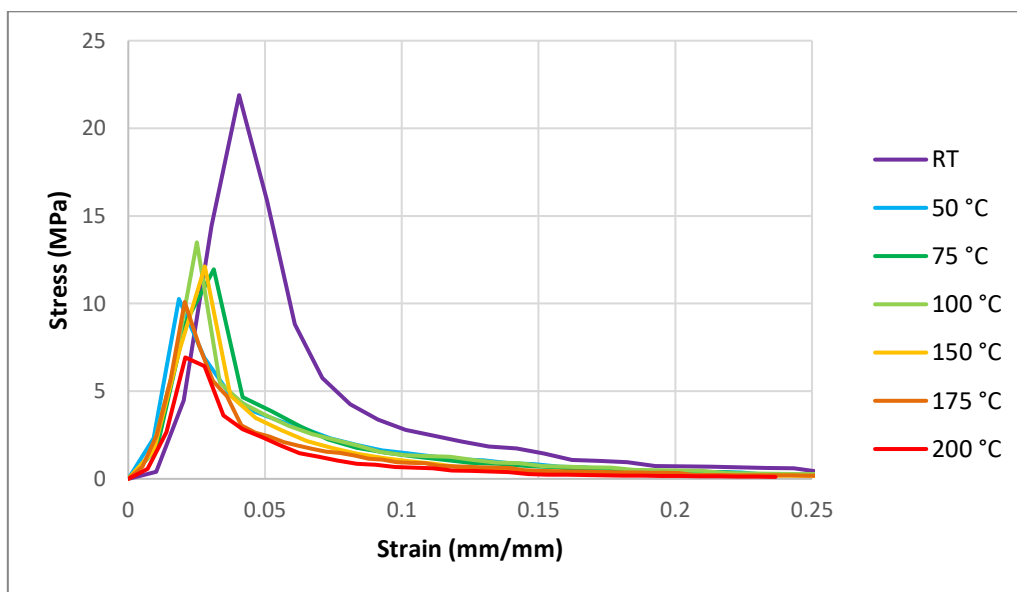


Figure 35: Stress-strain graph – Mechanical testing at 24 hours of cooling after heating

The rate of displacement of the loading mechanism was measured to be constant and within the range of 2.5 mm/s – 4.0 mm/s. With this range of displacement rate, it was observed that the failure load of the test specimens all occurred within the first two seconds of loading (strain in the range 0.02 mm/s – 0.05 mm/s). These failure loads directly correspond to the modulus of rupture (failure stress). This value corresponds to the peak observed in each stress-strain curve Figure 34 and Figure 35. Upon further subsection to displacement, the stress on the test specimens gradually reduced.

The failure stress of the OSB3 at different temperature levels is an important finding in this research work. Figure 36 and Figure 37 give a graphical representation of the failure stresses of the test specimens at different temperature levels. Figure 36 and Figure 37 provide data corresponding to the bending tests performed immediately upon removing specimens from the furnace and the bending tests performed 24 hours after removing the specimens from the furnace respectively.

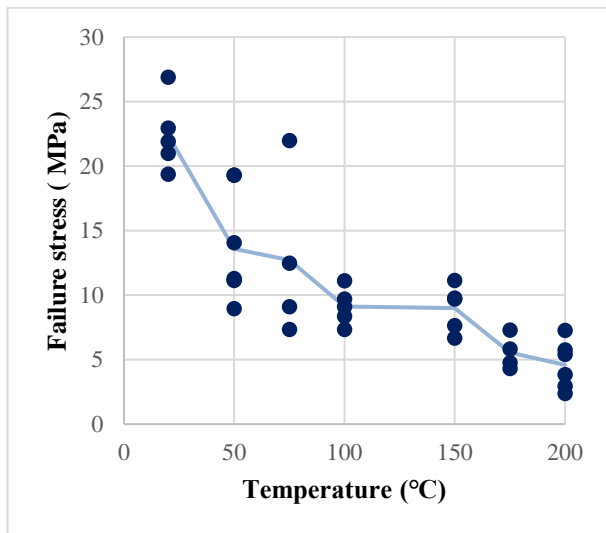


Figure 36: Failure stresses - Mechanical testing immediately after heating

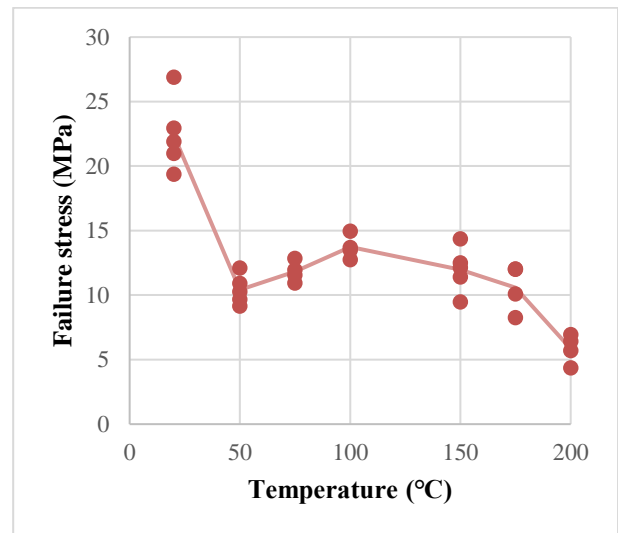


Figure 37: Failure stresses - Mechanical testing at 24 hours of cooling after heating

The mean values of the failure stresses at each temperature and the standard deviation of the results were calculated and are provided in Table 13. The mean failure stress for the OSB3 at room temperature conditions was calculated to be 22.4 MPa with a standard deviation of 2.8 MPa. The table also gives the average loss of strength for each test set relative to the average failure stress at room temperature. The strength regained during the 24-hour period of cooling was also calculated for each temperature and the results are included in the table.

For the bending tests conducted immediately upon removing the test specimens from the furnace, it can be observed that the average failure stress decreased with increasing temperature, although non-linearly. For the test temperature of 50 °C, the strength loss was 39.3%. In the range of 50 °C – 200 °C, major strength decreases are observed from 75 °C to 100 °C and 150 °C to 175 °C. In the temperature range of 100 °C – 150 °C, the strength decrease is observed to be at a minimum (0.6%). Another important observation for the test set is that for the specimen tests at room temperature, 50 °C, and 75 °C, the failure stresses have a larger

range size compared to other test temperatures. This is confirmed by the standard deviations of the test sets, as seen in Table 13.

For the bending tests conducted 24 hours after removing the test specimens from the furnace, the strength loss does not follow a similar pattern. There is a significant decrease in the failure stress for the 50 °C tests. For the following test temperatures of 75 °C and 100 °C, the failure stress increases, and then for the subsequent test temperatures of 150 °C, 175 °C, and 200 °C the failure stress decreases. Comparing the mean strength losses at different test temperatures, the strength loss for the 50 °C tests is the second-highest in the test set, only exceeded by the strength loss of the 200 °C tests.

Table 13: Average values for strength regained at 24 hours of cooling in the thermal-mechanical tests

Test temperature (°C)	Bending tests performed immediately upon removal from the furnace			Bending tests performed 24 hours after removal from the furnace			Strength regained at 24 hours
	Failure stress (MPa)		Loss of strength	Failure stress (MPa)		Loss of strength	
	Mean	Standard deviation		Mean	Standard deviation		
50	13.6	4.2	60.7%	10.4	1.1	46.5%	-14.2%
75	12.7	6.5	56.7%	11.8	0.8	52.7%	-4.0%
100	9.1	1.4	40.7%	13.7	0.9	61.2%	20.6%
150	9.0	1.8	40.1%	12.0	1.8	53.4%	13.3%
175	5.5	1.3	24.7%	10.6	1.8	47.3%	22.5%
200	4.6	1.9	20.5%	5.84	1.1	26.1%	5.6%

The tests results were also used to identify the strength regained during the 24-hour cooling period, relative to the original strength of the material. For the test temperatures of 50 °C and 75 °C, the calculations revealed negative values for the strength regained, meaning that during the 24-hour period, strength was further lost. For the 50 °C test temperature, strength loss was 14.2%, which is fairly significant. However, for the 75 °C test temperature, the strength loss was much smaller at 4%. For the higher test temperatures, the strength regained was calculated to have positive values, with the highest strength regain being for the 175 °C test temperature (22.5%).

5 Thermal Modelling Methodology

This section describes the methodology of the heat transfer simulation performed for the OSB3 material that was used in the experimental procedure. The heat conduction occurring in the OSB3 material during the cone calorimeter test was modelled. All simulations were performed using the “COMSOL Multiphysics®” software (version 5.3) [46].

5.1 Geometry and Heat Flux Boundary Condition

The heat transfer mechanism was modelled to predict temperatures and temperature distribution through the thickness of the assembly. The assembly consists of two OSB3 specimens of dimension 100 mm x 100 mm x 10.8 mm stacked on top of each other, then stacked on a piece of ceramic wool of dimension 100 mm x 100 mm x 10.0 mm similar to the cone calorimeter test performed previously. Figure 38 displays the heat transfer model used for the simulation, which follows a simplified version of the material setup in the cone calorimeter test. From the simulation, temperatures at points P1, P2, and P3 with change in time were obtained. The simulation was limited to the period of pre-ignition of the OSB3.

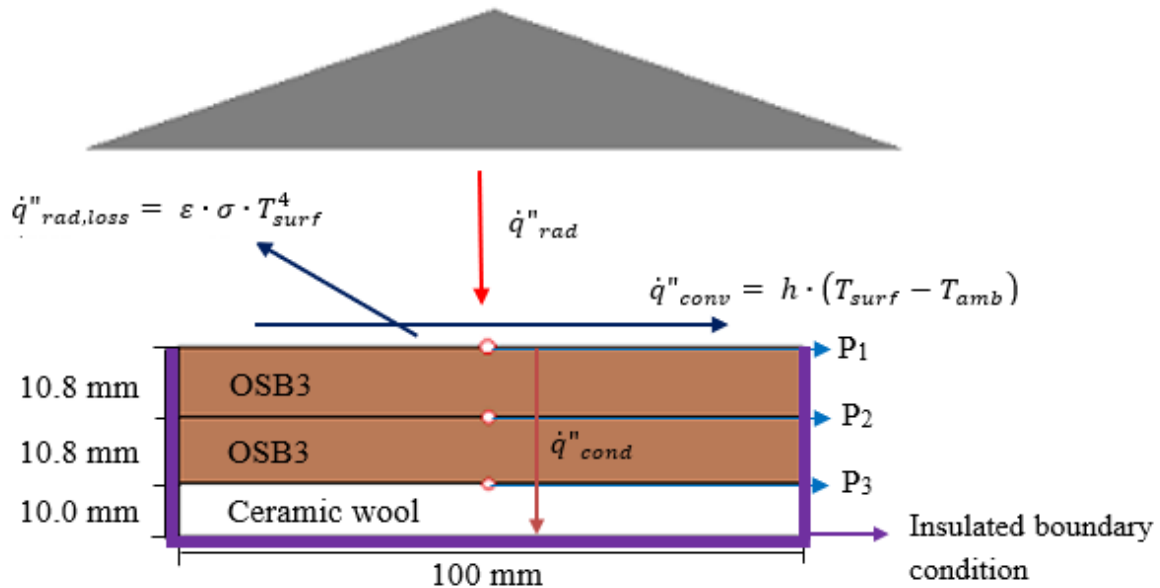


Figure 38: Heat transfer model used for thermal simulation

The model only considered the influx of heat on the top surface of the test specimen. The inward heat flux on the surface considered the radiant heat flux from the cone, radiant heat loss and convective heat loss. The net inward heat flux can be given by equation (7).

$$\dot{q}''_{net} = \dot{q}''_{rad} - \dot{q}''_{rad,loss} - \dot{q}''_{conv} \quad (7)$$

$$\dot{q}''_{net} = \dot{q}''_{rad} - \varepsilon \cdot \sigma \cdot T_{surf}^4 - h \cdot (T_{surf} - T_{amb})$$

The inward heat flux was limited to the top surface of the material setup by providing thermal insulation on the other five open surfaces.

The inward heat flux application and the thermal insulation on the heat transfer model are displayed by Figure 39 and Figure 40 respectively. The surfaces shaded in purple represent the impacted surfaces.

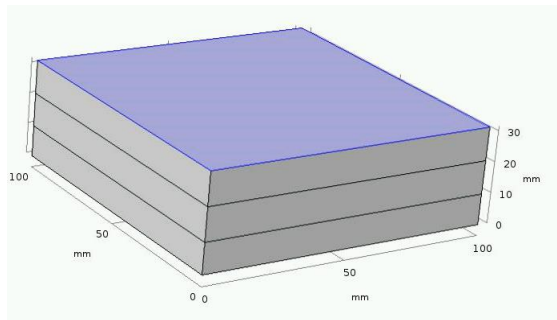


Figure 39: Heat flux boundary condition on the heat transfer model

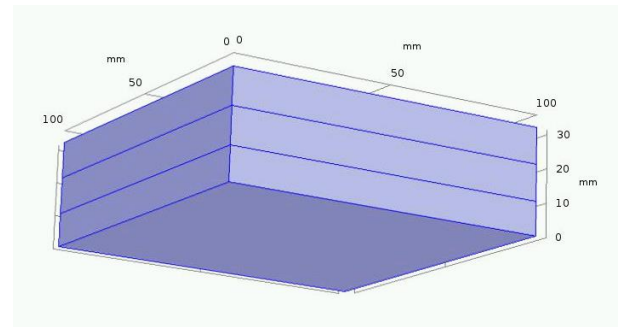


Figure 40: Thermal insulation on the heat transfer model

5.2 Material Data

Two material types were considered: OSB3 and ceramic wool. For these two materials, three material properties were given as the input for the heat transfer model: density, specific heat capacity at constant pressure, and thermal conductivity.

For the ceramic wool, these data were obtained from Kodur and Harmathy (2016) [47] and are given in Table 14. To simplify the model, the material properties' dependency on temperature was not considered for the ceramic wool.

Table 14: Material properties of ceramic wool

Density	Specific heat capacity	Thermal conductivity
150 kg/m ³	1200 J/kg/K	0.2 W/m/K

For OSB3, the density at ambient conditions was obtained from the specimen data used in the cone calorimeter test as 593.3 ± 20.1 kg/m³. For the material properties of specific heat capacity and thermal conductivity, temperature dependency was considered.

For the plot of specific heat capacity of OSB3 against temperature, the data given by EN 1995-1-2 (2004) [48] for timber was used. A correction was made for the peak around 373 K – 393 K, considering a moisture content of 5.2% for OSB3 (calculated in 4.2.2). The function as given by Figure 41 was used for the specific heat capacity of OSB3 in the heat transfer model.

Similarly, for the plot of thermal conductivity against temperature, the data given in EN 1995-1-2 (2004) [48] for timber was considered, along with the experimental data results. The thermal conductivity-temperature function given in the code was used to extrapolate the data obtained from the previously conducted thermal conductivity test to the temperature range of 80 °C – 1000 °C. The function as given by Figure 42Figure 41 was used for the thermal conductivity of OSB3 in the heat transfer model.

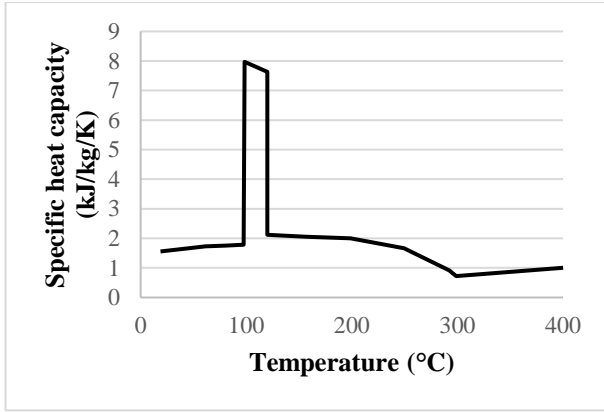


Figure 41: Plot of specific heat capacity of OSB3 against temperature

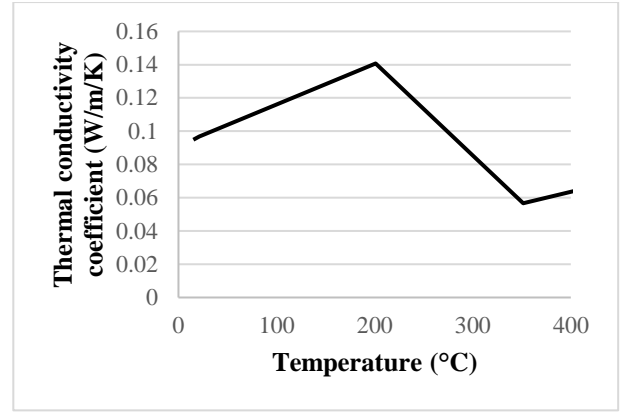


Figure 42: Plot of thermal conductivity of OSB3 against temperature

5.3 Simulation Settings

The focus of the simulations was pre-ignition heat conduction of OSB3. From the cone calorimeter tests, the test done using a radiant heat flux of 15 kW/m^2 had a delayed ignition time. For this reason, the simulations used a radiant heat flux value of 15 kW/m^2 . Other dependent parameters used in the heat transfer model include convective heat transfer coefficient, emissivity, ambient temperature, and initial temperature of the material. The emissivity value was taken as 0.91 (given for timber, planed) [49]. The ambient temperature and the initial temperature of the materials were kept at $20 \text{ }^\circ\text{C}$.

Three different simulation settings were run using the heat transfer model.

- Scenario 1: $h = 13.5 \text{ kW/m}^2/\text{K}$ (data from [50])
- Scenario 2: $h = 15 \text{ kW/m}^2/\text{K}$ (data from [51])
- Scenario 3: Instead of defining an inward heat flux at the top surface, a temperature curve was defined for the top surface generated from the data of the cone calorimeter. The temperature curve is given by Figure 43.

For each simulation, an extra-fine mesh was built as shown by Figure 44. Each simulation was run for a period of 1100 seconds.

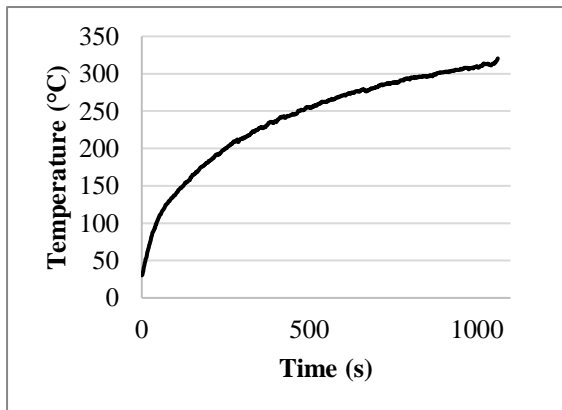


Figure 43: Temperature-time curve of top surface from cone calorimeter data

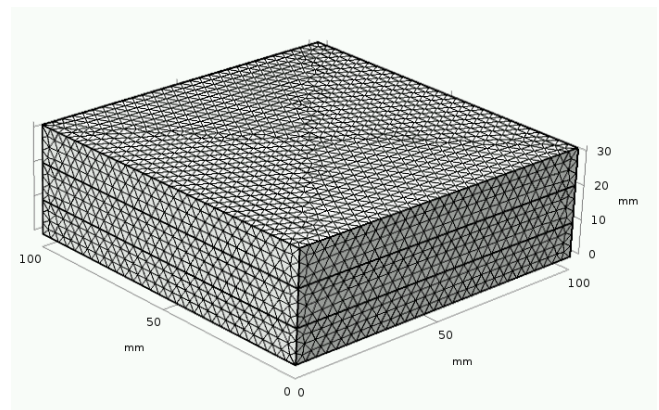


Figure 44: Mesh setting in heat transfer model

6 Thermal Modelling Results

This section describes the results of the simulation of the heat transfer through OSB3. The main result is the temperature-time curves for each simulation scenario.

6.1 Simulation Scenarios with Input of Heat Flux Boundary Condition

Two simulation scenarios were run using the inward heat flux model, varying only the parameter of convective heat transfer coefficient. Figure 45 and Figure 46 refer to the simulation scenario with an h value of $13.5 \text{ kW/m}^2/\text{K}$ and Figure 47 and Figure 48 refer to the simulation scenario with an h value of $15 \text{ kW/m}^2/\text{K}$.

By comparing the figures, it is clear that the difference between the results of the two scenarios are minute. Simulation scenario 1 has final temperature values at points P1, P2, and P3 that are slightly higher than the corresponding values in simulation scenario 2. Considering the temperature-time curves of the top surface, it can be observed that the curve has a trend similar to a logarithmic curve. The rate of temperature increase is initially very high and decreases with increasing time. After a period in the range of 800 s, the rate of temperature increased at the surface is observed to be minimal. The final temperature at 1100 s was recorded to be $357 \text{ }^\circ\text{C}$ and $349 \text{ }^\circ\text{C}$ for simulation scenarios 1 and 2 respectively.

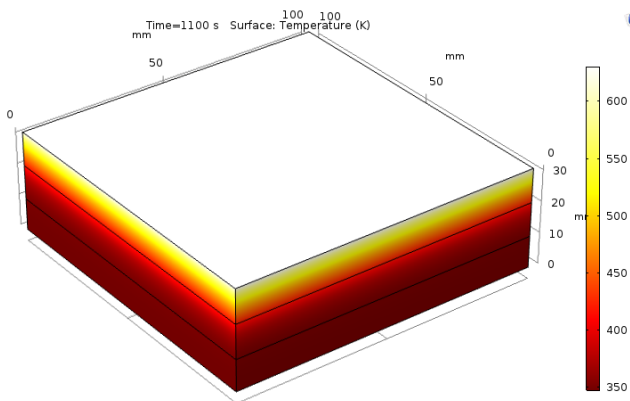


Figure 45: Surface temperature at 1100 s – Simulation scenario 1

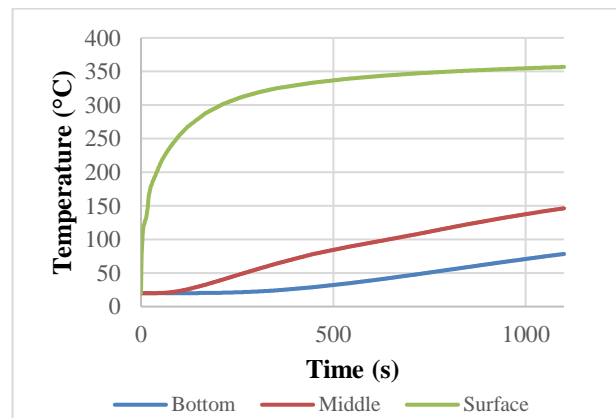


Figure 46: Temperature-time curves – Simulation scenario 1

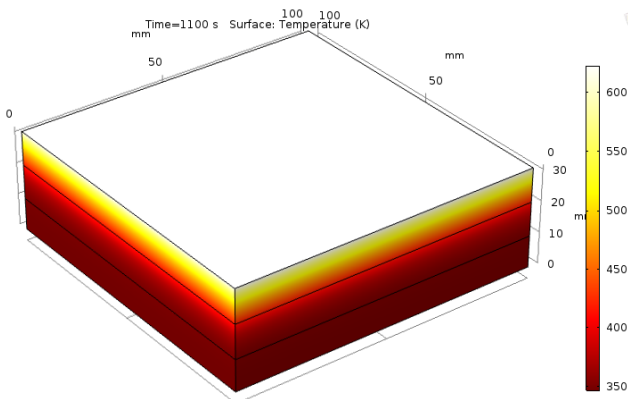


Figure 47: Surface temperature at 1100 s – Simulation scenario 2

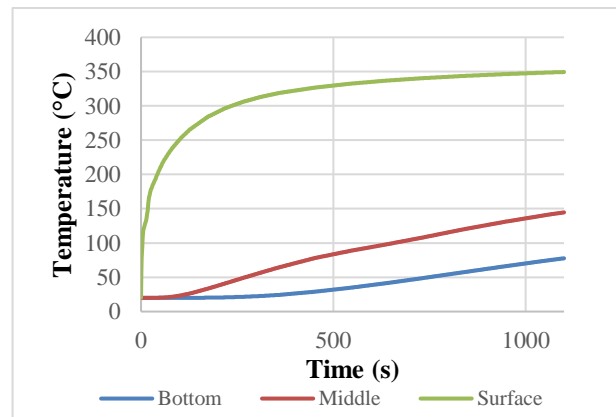


Figure 48: Temperature-time curves – Simulation scenario 2

The temperature-time curves for the middle and bottom of the OSB3 completely differ from the surface curve but are somewhat similar to each other. The initial rate of temperature increase in both curves is near zero and increases until a time in the range of 500 s. After that time, the rate of temperature increase looks to be at a constant level. At the end of 1100 s, the temperatures in the middle and bottom of the material were recorded to be 78 °C and 146 °C for scenario 1 and 78 °C and 145 °C for scenario 2 respectively.

6.2 Simulation Scenarios with Input of Prescribed Temperature Boundary Condition

In the third simulation scenario, the input was the temperature-time curve at the top surface of the material, based on the temperature recording of the cone calorimeter test. Figure 49 and Figure 50 refer to this simulation scenario. The temperature-time curve of the surface is a repetition of the input data. However, comparing the temperature-time curves of the middle and bottom, it is observed that the trends of the curves are somewhat similar to the corresponding curves in scenarios 1 and 2. At the end of 1100 s, the temperatures in the middle and bottom of the material were recorded to be 65 °C and 121 °C

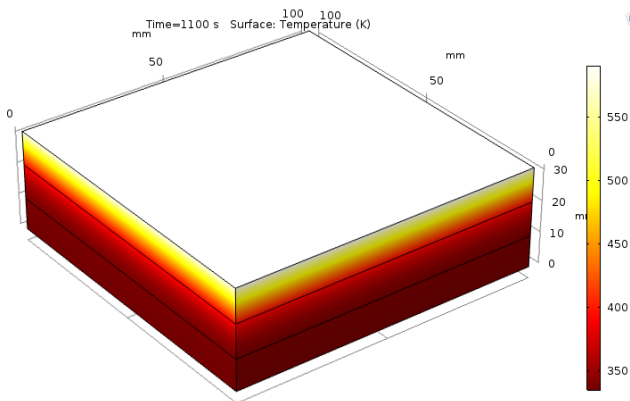


Figure 49: Surface temperature at 1100 s – Simulation scenario 3

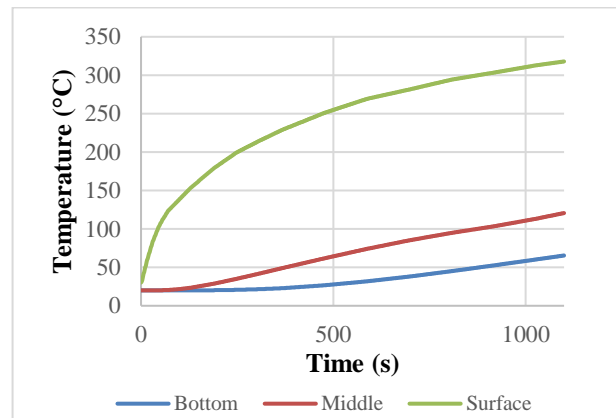


Figure 50: Temperature-time curves – Simulation scenario 3

6.3 Comparison of Simulation Results with Experimental Measurements

The results of the three separate simulation scenario runs performed for the thermal modelling were compared with the experimental measurement taken during the cone calorimeter tests. The simulation results and experimental results have been plotted in Figure 51, Figure 52, and Figure 53 for simulation scenarios 1, 2, and 3 respectively.

In Figure 51 and Figure 52, it is clearly observed that the temperature-time curves for the simulations and experimental measurements of the OSB3 material surface are significantly different. At the end of 1000 s, there is almost a difference of 50 °C between the experimental and simulation temperatures of the OSB3 surface.

For the middle temperature reading, the temperature-time curves for the experimental and simulation data follow a similar pattern, with the temperature difference at the point with the largest variation being about 15 °C. Around the time the temperature reaches 100 °C, a

flattening of both curves is seen. This can be attributed to the moisture vaporization observed in the material around this temperature.

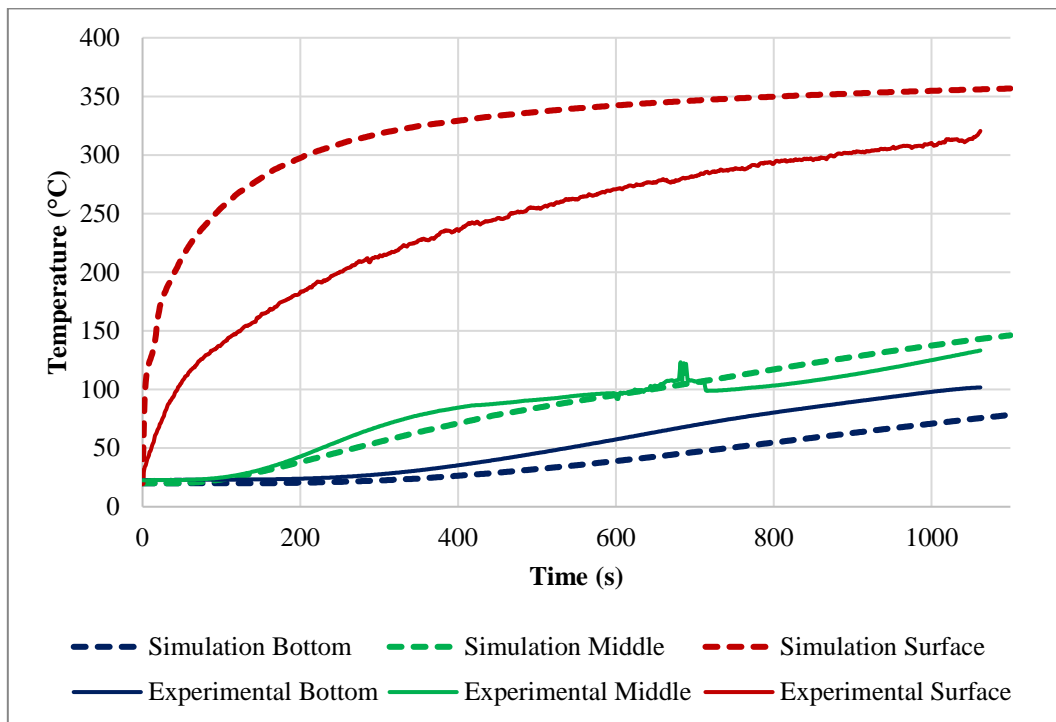


Figure 51: Comparison of simulation scenario 1 results with experimental measurements

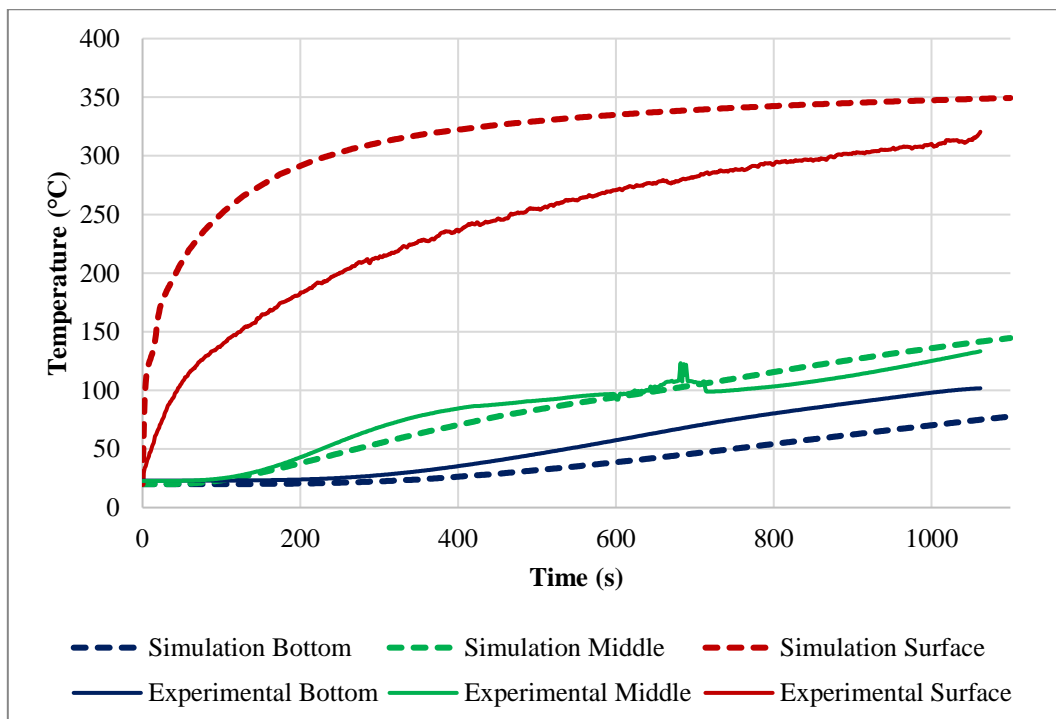


Figure 52: Comparison of simulation scenario 2 results with experimental measurements

When considering the temperature-time curves for the bottom of the material in the simulation and experimental results, the trends of both curves are similar. Until around 200 s, both curves have minimal temperature increase, after which a slow increasing gradient is observed. At

around 800 s, the temperatures of the simulation (1 and 2) and experimental curves are roughly 55 °C, 55 °C and 80 °C respectively. Onwards from 800 s until 1000 s, both curves are parallel, keeping the temperature difference at a constant level.

In both figures, at the end of the common observed time (1062 s), the experimental temperatures are lower than the simulation temperatures for the surface and middle, but higher for the bottom of the material.

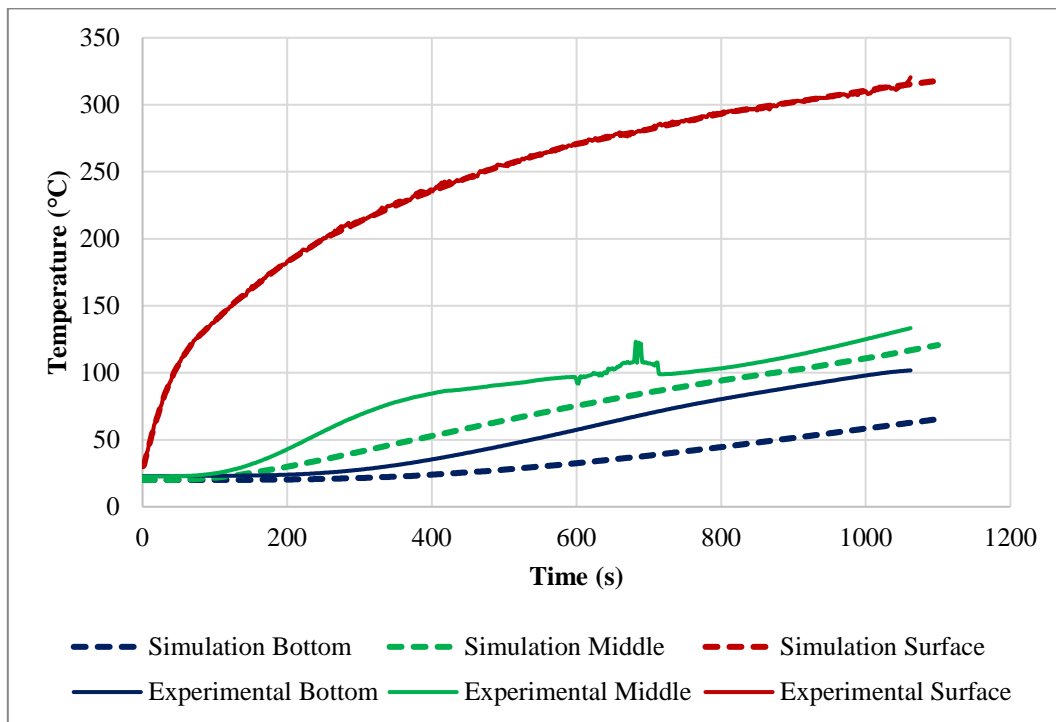


Figure 53: Comparison of simulation scenario 3 results with experimental measurements

When comparing the temperature-time curves of the simulation of scenario 3 (input of surface temperature-time curve) with the experimental results (Figure 53), it is seen that the middle and bottom temperature-time curves have a similar trend to those of the simulations 1 and 2. But the rate of temperature increase is not as high as those observed in the previous simulation results. This is to be expected, as the surface temperature-time curve for simulation 3 behaves at a much slower pace than the surface temperature-time curves for simulations 1 and 2.

For the middle temperature-time curves, during the entire simulated time, the experimental temperature is observed to be higher than the simulation temperatures. The flattening of the curve observed due to the moisture vaporization from the material appears to occur at an earlier stage for the experimental values than for the simulated results.

For the bottom temperature, the trends of both experimental and simulation temperature-time curves are similar. Until around 200 s, both curves have minimal temperature increase, after which a slow increasing gradient is observed. At around 800 s, the temperatures of the simulation and experimental curves are roughly 44 °C and 80 °C respectively. Onwards from 800 s until 1000 s, both curves are parallel, keeping the temperature difference at a constant level.

7 Discussion

This thesis work contained a number of experimental and computational activities regarding the performance of OSB3 at high thermal conditions. The work investigated the thermal and mechanical behavior of the material. The purpose of this section is to analyze these results and compare them with related work done by other researchers in the past to further increase the understanding of the behavior of OSB.

7.1 Thermal Decomposition of OSB

The material decomposition of OSB3 was investigated using the TGA tests at a temperature range of 20 °C – 400 °C. A minimal mass loss of $1.9 \pm 0.1\%$ was observed at 225 °C. From 225 °C to 400 °C, there was a significant drop in mass, with the remaining mass being $31.3 \pm 0.4\%$ of the initial mass. Additionally, by considering the mass losses at temperatures around 95 ° - 110 °C, the moisture content of the material was identified to be 0.55%.

Similar studies by Yapici (2020), Ira et al. (2020), and Gong et al. (2021) analyzing OSB using TGA gave similar results (seen in Table 4) [6], [31], [33]. The major difference observed between literature and experimental results is the mass loss observed at around 100 °C (4% for Yapici (2020), 5% for Ira et al. (2020), and 2% for Gong et al. (2021)). This mass loss can be attributed to the moisture content of the timber composite. Considering this, the mass loss at 100 °C in the TGA test will depend on the moisture content present.

The moisture content of OSB can range between approximately 0 % - 10 % depending on the manufacturer's specifications [38], but is typically found to range between 2% - 8%. However, according to the results of the TGA tests conducted, the calculated moisture content ranged from 0.21% to 0.89%. This is a very low moisture content for a timber product, and it questions the sensitivity of the TGA results at such low mass losses. Although it is not visible in the complete mass loss-time graph, there is a slight mass increase (above 100%) at the start of each TGA test. This is generally attributed to the buoyancy caused by the flow of gases in the test. To confirm the accuracy of the moisture content calculations from the TGA test, they need to be compared with moisture loss calculated in other ways, such as the calculations done using the furnace-heating test data. The furnace-heating tests gave a moisture content of 5.2%, which is much greater than the TGA calculations and is more within the expected moisture content range of OSB.

Another finding of the TGA results is that thermal degradation depends on the heating rate as well as the temperature. With an increase in the rate of heating, the time taken to reach a temperature point decreases. This translates to any specific mass loss occurring at a relatively higher temperature value for a higher heating rate. The mass loss rate in the range where significant mass loss occurs is also higher for any specific mass loss for a test at a higher heating rate.

7.2 Thermal Properties of OSB

This sub-section will discuss the results of the thermal conductivity and cone calorimeter tests performed.

7.2.1 Thermal Conductivity

Results of the thermal conductivity test performed for OSB3 in the temperature range of 15 °C – 84 °C generated a linear relationship between the material's thermal conductivity and temperature (equation (2)).

$$k = 2.44 \times 10^{-4} \times T(^{\circ}\text{C}) + 0.09168 \quad (2)$$

The average value of thermal conductivity was 0.1 W/m/K, which is equivalent to the results seen in the work of Sonderegger and Niemz (2009) and Vololonirina et al. (2014) [35], [37].

However, it is important to understand that this linear relationship should not be extrapolated to higher temperatures. According to EN 1995-1-2 (2004), the linear increase of thermal conductivity with temperature in timber only occurs until 200 °C, upon which the relationship between thermal conductivity and temperature changes [48]. Further changes are observed at 350 °C, 500 °C, and 800 °C (considering the temperature range of 20 °C – 820 °C). These changes may be linked to ignition and charring phenomena seen in wood. A suggestion can be made that those similar changes could be observed in the thermal conductivity of OSB as a function of temperature.

7.2.2 Cone Calorimeter Tests

The cone calorimeter tests performed gave a CHF value of 14.6 kW/m² for OSB3. The result is comparable to the CHF result of 16.7 kW/m² in Rantuch et al. (2015) [27]. The tests were performed for three different radiant heat flux values, with at least one repeat test performed for each radiant heat flux. The objective of the repeat tests was to investigate the repeatability of the test results. Since OSB is not a homogeneous material and the size of the cone calorimeter test specimens is very small, repeatability of test results was a point of concern. Two important results of the cone calorimeter tests were compared: time to ignition and peak HRR. For most of the tests, repeatability was observed in the results (Range size: Peak HRR: 2 kW/m², 62 kW/m², 3 kW/m² and t_{ig} : 18 s, 33 s, 1 s for \dot{q}_{rad} : 15 kW/m², 25 kW/m², 35 kW/m² respectively).

For the test set performed with the radiant heat flux of 25 kW/m², the time to ignition and peak HRR in the first test was observed to be significantly higher compared to the other two tests. However, considering the specimen preparation in the holder, the first test in the radiant heat flux of 25 kW/m² test set was the only time a metal wire mesh was not used above the OSB3 surface. This allowed more freedom for the test specimen, which may have led to different behavior compared to the other tests and comparatively higher results.

The experimental results were compared with similar studies found during the literature survey considering the peak HRR and time to ignition. Table 15 and Table 16 are a compilation of both the experimental and literature data for the peak HRR and time to ignition respectively. For the radiant heat flux values in the range of 20 kW/m² – 50 kW/m², the cone calorimeter gave results of peak HRR in the range of 163 kW/m² – 234 kW/m². For the lowest radiant heat flux value of 15 kW/m², the peak HRR of the cone calorimeter test was observed to be much lower at 121 ± 1 kW/m². Similarly, for the higher radiant heat flux values ranging from 60 kW/m² – 80 kW/m², the peak HRR of the cone calorimeter test was observed to be at a

higher range than mentioned above at 234 kW/m² - 337 kW/m². As can be seen, exact overlap in experimental conditions between the experiments conducted as part of this these and previously published results is only found for 35 kW/m², but in this case the agreement is good.

Considering the time to ignition across the different experimental and literature results, the values vary slightly for each radiant heat flux.

Table 15: HRR_{peak} value comparison between experimental and literature results

\dot{q}_{rad}'' (kW/m ²)	Experimental results (kW/m ²)			White and Winandy (2006) [26] (kW/m ²)			Rantuch et al. (2015) [27] (kW/m ²)	Ira et al. (2020) [31] (kW/m ²)
	Test 1	Test 2	Test 3	Type A	Type B	Type C		
15	122	120	-	-	-	-	-	-
20	-	-	-	169	193	171	209	203
25	227	197	165	-	-	-	-	-
30	-	-	-	-	-	-	196	-
35	164	161	-	163	164	181	-	-
40	-	-	-	-	-	-	210	-
50	-	-	-	198	191	218	234	250
60	-	-	-	-	-	-	301	-
65	-	-	-	252	234	284	-	-
80	-	-	-	-	-	-	-	337

Table 16: t_{ig} value comparison between experimental and literature results

\dot{q}_{rad}'' (kW/m ²)	Experimental results (s)			White and Winandy (2006) [26] (s)			Rantuch et al. (2015) [27] (s)	Ira et al. (2020) [31] (s)
	Test 1	Test 2	Test 3	Type A	Type B	Type C		
15	1080	1062	-	-	-	-	-	-
20	-	-	-	195	306	157	138	188
25	138	105	108	-	-	-	-	-
30	-	-	-	-	-	-	49	-
35	53	52	-	39	66	43	-	-
40	-	-	-	-	-	-	24	-
50	-	-	-	19	20	16	17	21
60	-	-	-	-	-	-	13	-
65	-	-	-	10	13	11	-	-
80	-	-	-	-	-	-	-	16

Another factor to be considered when studying OSB is that similar to different types of time, different types of OSB types perform differently in terms of factors such as time to ignition and peak HRR. This factor is clearly observed when comparing the results of White and

Winandy (2006) [26], where the major difference between the three OSB types was the type of timber used to produce the timber composite.

7.3 Thermal Decomposition and Mechanical Degradation of OSB

Natural timber has a major axis and minor axis, with the strength being higher parallel for the major axis. Although this strength disparity between the two axes is reduced in OSB, the material still has a defined major axis and a minor axis. Each bending test in this experimental procedure was carried out for the major axis of the OSB3.

From the material information given by the manufacturer, the bending strength of the OSB3 panel used (thickness 11 mm) is 20 MPa for the major axis. The bending tests performed for five OSB3 specimens at room temperature (20 °C) gave an average value of 22.4 MPa for the failure stress (equivalent to the bending strength). The experimental results closely match the minimum bending strength value provided by the manufacturer for the OSB3 material.

The experimental results were compared with past studies performed for OSB by Bekhta et al. (2003) [41] and Sinha et al. (2011) [10] considering the failure stress values. These results are plotted against each other in Figure 54 and Figure 55 for the bending tests conducted immediately upon the removal of specimens from the oven and for the bending tests performed after 24 hours of cooling respectively.

The data taken from past studies consider specimens kept in a steady-state temperature for a uniform time period. However, the experimental work was performed for the time taken for the specimen center to reach a steady-state temperature with the addition of one hour. However, for comparison, the average time the specimens were kept in the furnace, two hours, is considered.

For the bending tests performed on OSB3 immediately upon removal from the furnace, the results were compared against the results of Bekhta et al. (2003). The past study only kept the specimens in a furnace for one hour, so it is to be expected that any loss of strength would be lower than for the experimental results. Unlike in the past study, a significant strength drop was observed in the 50 °C temperature experimental results. Considering the temperature range of 60 °C – 140 °C tests, gradual loss of strength was observed in both works, although the pattern of descent was not exactly replicated.

For the bending tests performed on OSB3 after 24 hours of cooling, the results were compared against the results of Sinha et al. (2011). The comparison of the two works provides significantly different trends for the failure stresses for most of the range. However, in the temperature range of 150 °C – 200 °C, a gradual decrease of strength was observed in both the past study and the experimental work.

An important finding from the test result set of bending tests on OSB3 after 24 hours of cooling is that after the failure stress drops for the 50 °C test temperature, an increase in failure stress is observed up to 100 °C, after which the failure stress drops at a much lower gradient until 175 °C. From 175 °C to 200 °C, the failure stress decreases more significantly. Although this trend

of failure stress of OSB3 is not similarly observed in the work done by Sinha et al. (2011), a similar pattern is seen in the study by Reszka and Torero (2016) [34] for timber.

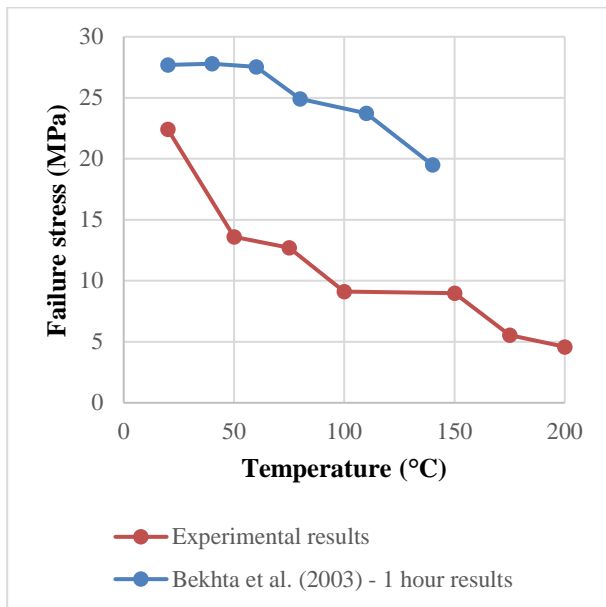


Figure 54: Comparison of experimental results with results of Bekhta et al. (2003) - Mechanical testing immediately after heating

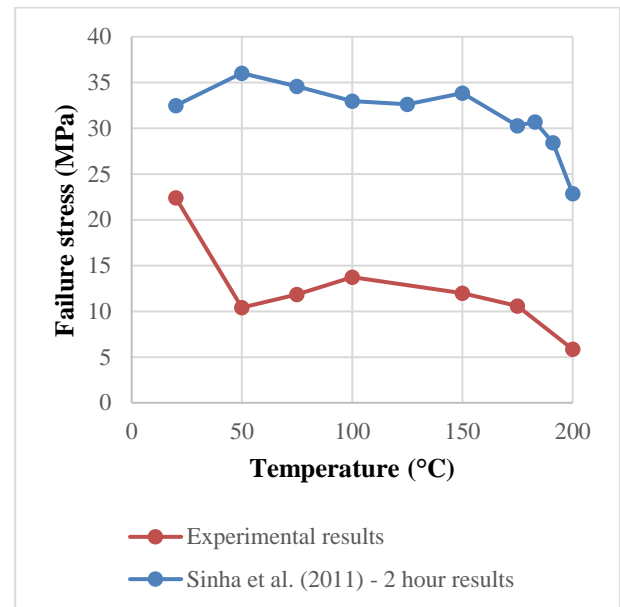


Figure 55: Comparison of experimental results with results of Sinha et al. (2011) - Mechanical testing at 24 hours of cooling after heating

The shape of the failure stress-temperature curve can be explained by the following theory. When the moisture content of timber is reduced, an increase in the strength of timber is observed. This explains the increase in failure stress in the test temperatures of 75 °C and 100 °C. It is noted that a similar increase is not observed for bending tests performed immediately after removing the specimens from the furnace. This could be due to the weakness in the adhesive while the sample is still hot, and so the moisture content will not have a similar impact at that point.

At temperatures of 150 °C and above, significant pyrolysis will occur in the timber, which can permanently reduce the strength. This could be the reason for similar patterns of strength loss for both bending test types (immediately after removal from the furnace and after 24 hours of cooling) in the temperature range of 150 °C – 200 °C. When comparing strength decrease, compressive strength decrease is usually higher than tensile strength decreases in the initial decrease. In bending tests, both compression and tension effects are felt by the material. Considering the higher severity of compressive strength loss, it is theorized that the failure stresses in the bending tests are compressive failure stresses.

The thermal-mechanical combination tests kept a limitation on the specimen material size. As OSB is a non-homogeneous material, to obtain a better representation of the material behavior, a larger specimen size would be better. However, the size of the specimen was limited considering the maximum allowance of the load cell and the maximum span allowance of the bending test rig.

7.4 Variations between Heat Transfer Simulation Results and Cone Calorimeter Experimental Measurements

The simulation results in Figure 51 and Figure 52 relate to the simulations run considering the input of the inward heat flux equation (7).

$$\dot{q}''_{net} = \dot{q}''_{rad} - (\dot{q}''_{rad,loss} - \dot{q}''_{conv}) \quad (7)$$

The simulation results in Figure 53 relate to the simulation run considering the input of the surface temperature-time curve as measured during the cone calorimeter test.

In all three simulation results, significant differences were observed between them and the experimental measurements. Reasons for these differences are discussed below focusing on the experimental measurements as well as the heat transfer model used in the simulations.

The temperature measurements in the cone calorimeter were done using type k thermocouples attached to the surface, middle and bottom of the OSB3 test specimen. Although the expectation in using a thermocouple is to measure the temperature of the attached surface, in reality it measures the temperature of the thermocouple itself. Therefore, it is necessary to understand the temperature measurements taken may have some deficiency in representing the actual temperature of the designated point.

From the comparison of the experimental results with the simulation results (simulations with input of inward heat flux equation), it is clearly observed that the temperature increase in the experimental data is much slower compared to the simulation results of the top surface. However, the inner thermocouples are predicted much better in the simulations.

Thermocouple reading errors could possibly be explained by considering that there may be a time delay in heating the thermocouple. The time taken to heat the thermocouple will depend on the mass of the thermocouple. The delay time identified can affect the thermocouple readings. However, the thermocouples used were type k thermocouples, with a low mass, meaning that the delay mentioned earlier would be minor. A more important factor to affect the thermocouple readings is the thermal contact between the thermocouple and the surface. At increasing temperatures, the thermocouple can detach from the surface. The contact between the thermocouple and the surface is important in determining whether the surface temperature is well represented. Also, to be considered is heat loss from the thermocouples that is not considered in the heat transfer model.

The above explanation could also explain the measured ignition temperatures of the OSB3 surface for the cone calorimeter tests as given by Table 10. It was observed that for higher heat fluxes, the measured surface ignition temperature had significantly lower values. Therefore, it can be theorized that this observed surface ignition temperature variation may be due to errors in the thermocouple readings. For higher heat fluxes, the time to ignition is lower, meaning inaccuracies from the thermocouple readings will have a higher impact on the thermocouple readings' accuracy.

An important note in the experimental results is the flattening of the middle temperature-time curve observed in the temperature range of 80 °C – 120 °C. This can be attributed to the evaporation of the moisture present in the material. A similar flattening was not observed in the simulation temperature-time curves, meaning the impact of moisture content in the sample has not been fully represented in the thermal properties such as specific heat capacity in the thermal model.

Another point in this subsection concerns simulation scenario 3, where a temperature boundary (based on experiment measurements) was applied on the exposed surface instead of the heat flux boundary. The aim of this was to analyze whether the experimental measurements were reasonable by comparing the temperature-time curves of the middle and bottom for both experimental measurements and simulation results. From the discussion of the above paragraphs, and the analysis of the graph plotted for the experimental and simulation results, it is suggested that the experimental measurements are not within a reasonable range to use as a temperature boundary application on the heat transfer model. This proves that the hypothesis to use the surface temperature-time curve from the experimental measurements as the boundary condition to emulate the heat conduction in the OSB3 was incorrect.

The final point to note in this subsection is regarding the thermal material property values used for OSB3, specifically the thermal conductivity coefficient and the specific heat capacity. These two properties need to be expressed as a function of temperature, as they are temperature-dependent. For the thermal conductivity coefficient, experimental results for OSB3 only yielded values up to a temperature of 84 °C. Considering the specific heat capacity of OSB, no temperature correlations were identified during the literature survey. This prompted the use of thermal conductivity coefficient-temperature and specific heat capacity-temperature plots given by the Eurocode 5 for natural timber in the simulations. This means that any impact of the adhesives on these thermal properties has been neglected. This could have also affected any variations found in the simulation results.

When adjusting the specific heat capacity-temperature plot of timber for OSB3, the main adjustment was made for the moisture content of OSB3. By using a moisture content value of 5.2% for the OSB3 (calculated in 4.2.2), the impact of the latent heat of vaporization of water (2.25×10^6 J/kg) on the specific heat capacity of the OSB3 material was adjusted over the temperature range of 100 °C – 120 °C.

In the simulations, the thermal properties of ceramic wool were applied constant values, without considering the impact of temperature. From the temperature-time curves, it can be deduced that the temperature change in the ceramic wool over the simulated time (1100 s) was in the range of 20 °C – 100 °C in both simulation and experimental results. Considering this, it can be suggested that any change in thermal properties of ceramic wool in this temperature range would be minimal and the impact on the simulation results by keeping the values constant would also be small.

By the overall analysis, it can be agreed that the heat flux boundary condition simulations (scenarios 1 and 2) can be considered appropriate for the heat transfer model. Still, there were

small inconsistencies seen between the experimental and simulation temperature-time curves, which means that there could be some inaccuracy of the thermal property representation of OSB3 in the model. To analyze a better fitting temperature-time curve, it might be prudent to perform a sensitivity study changing relevant inputs such as specific heat capacity, thermal conductivity and ambient temperature.

7.5 Barriers to Comparison of Results

The classification of OSB considers the mechanical strength of the material, which is one of the most important parameters in construction. Considering that OSB can be manufactured with different types of timber, the classification is helpful when comparing data from experimental and literature data. If the material classification is known, not only mechanical strength but also other material properties of an OSB product of a certain classification can be compared with only other OSB products of the same classification. This could be helpful when validating material data with data from the literature. Most of the research studies performed for OSB that were compiled in the literature review do not mention the classification of OSB that was studied. This generates a significant limitation in the comparison of experimental results with results found in the literature.

8 Summary and Conclusions

The goal of this research work was to contribute the knowledge and understanding of thermal decomposition and mechanical degradation of OSB. Structural failure of engineered timber in relation to high temperatures and fire occurs in one of two different ways:

- Thermal degradation of material properties of timber can cause diminished mechanical strength.
- Charring can cause a reduction of the element cross-section leading to increased loading pressure.

In this research work, the scope was limited to pre-ignition behavior of OSB. Therefore, only the decrease of mechanical strength with thermal degradation of the material is considered here.

The research work is a combination of experimental and computational studies, designed to achieve three defined objectives with regard to OSB3. The summarization of the research work findings is listed below.

- The first defined objective was to analyze the thermal decomposition of OSB3 and related thermal material properties. Thermal material property tests (TGA, thermal conductivity test, and cone calorimeter tests) were performed for OSB3. The TGA tests were carried out under 100% nitrogen atmosphere in the temperature range of 20 °C – 400 °C and avoided the occurrence of combustion occurring. The tests identified only a mass loss of 1.9 % until the temperature of 225 °C was reached. In the next temperature range 225 °C – (380 ± 10) °C, mass percentage decreased significantly up to 32%. The thermal conductivity test identified an average value of 0.1 W/m/K for the thermal conductivity coefficient in the temperature range 15 °C – 84 °C and a linearly increasing thermal conductivity coefficient-temperature relationship. The cone calorimeter tests identified a CHF value of 14.6 kW/m² for OSB3 and peak HRR values in the range of 164 kW/m² – 227 kW/m² for radiant heat fluxes of 25 kW/m² and 35 kW/m². However, for the tests at a lower radiant heat flux of 15 kW/m², the observed peak HRR was much lower at an average value of 121 kW/m².
- The second defined objective was to investigate any possible correlation between thermal decomposition and mechanical degradation of OSB3. The experimental procedure planned for OSB3 specimens to be placed in a furnace at a defined steady-state temperature for the time of one hour + time taken for the specimen center to reach the furnace temperature and subject them to a three-point bending test upon removal from the furnace, either immediately or after 24 hours of cooling. For the specimen tests performed immediately upon removal from the furnace, the failure stress decreased with increasing test temperatures from room temperature to 200 °C in a non-linear pattern. Changing from 100 °C to 150 °C, the decrease in failure stress was minimal. For the specimen tests performed after 24 hours of cooling, the failure stress pattern was somewhat different from the other test set. After a significant drop in failure stress from room temperature to 50 °C, the failure stress increases with the increase in

test temperature from 75 °C to 100 °C. For the test temperatures following 100 °C, the failure stress decreased again. Comparing the failure stresses of specimens tested immediately after removing from the furnace and the specimens tested after 24 hours of cooling, it was observed that in the cooling period, strength was regained was specimens heated at 100 °C, 150 °C, 175 °C, and 200 °C.

- The third defined objective was to perform heat transfer modelling of OSB3 using data obtained from the experimental work and the literature study. The heat transfer model of the cone calorimeter test was replicated. Simulations were run either by applying a heat flux boundary on the exposed surface or a temperature surface. The simulation results from the model applying a heat flux boundary on the exposed surface produced temperature-time curves similar to the thermocouple recording taken in the cone calorimeter test. However, possible inaccuracies in the thermocouple readings were identified meaning that the readings could not be effectively used to validate the simulation results.

The main conclusions of this thesis work can be identified as given below.

- The thermal decomposition (mass loss) of a timber product like OSB can be different in the case of a microscale test like TGA and a small-scale test like furnace testing.
- The mechanical strength of OSB can experience degradation when exposed to long periods of high temperatures.
- For exposure temperatures of 100 °C – 200 °C, a cooling period after exposure lets the OSB regain a portion of the lost strength.
- At exposure temperatures of 100 °C – 175 °C, the loss of moisture in the OSB will contribute to an increase in strength.
- In thermal modelling, it is important to judge whether a) the boundary conditions are appropriate, b) thermal properties such as thermal conductivity coefficient, specific heat capacity, and density are correct, and c) the heat transfer model is correct.
- When trying to validate simulation results with experimental results, any inconsistencies in experimental data must be considered.

These findings confirm the research hypothesis of the correlation between thermal decomposition and mechanical degradation of OSB, as well as strength regain of OSB with a cooling period after heating. The findings of this research work can be used to predict the behavior of OSB3 panels used in construction at moderately high-temperature conditions (pre-ignition conditions). By identifying the thermal and mechanical points of weakness of the material, further studies can be performed to investigate methods of increasing temperature-dependent mechanical resistance of the material such as fire-retardant coatings for timber products.

9 Further Research

Suggestions can be made for the investigation of the following topics in order to expand on the knowledge gathered in this thesis.

- Investigation of the behavior of thermal material properties of OSB (such as thermal conductivity coefficient and specific heat capacity) along a larger range of temperatures.
- Expansion of the thermal degradation study of OSB to the individual materials present in OSB (wood materials; cellulose, hemicellulose, and lignin; and adhesives)
- Investigation of mechanical strength degradation of OSB in the minor axis with thermal decomposition. Comparisons may be made between the behavior in the major and minor axes.
- Comparison of mechanical strength degradation-thermal decomposition relationship of OSB with other timber composite panels used for similar uses such as plywood.
- Expansion of the performed mechanical strength degradation-thermal decomposition study of OSB to a higher temperature range.
- Investigation of the fire performance on OSB and the effect on the mechanical strength of OSB from fire.

10 References

- [1] A. R. Pearce, Y. H. Ahn, H. Co, and Ltd, *Sustainable Buildings and Infrastructure: Paths to the Future*. London: Routledge, 2012. doi: 10.4324/9780203130841.
- [2] B. J. Meacham *et al.*, ‘Quantification of Green Building Features on Firefighter Safety - Year 1 Report’, 2014, doi: 10.13140/RG.2.2.19096.34563.
- [3] J. Elkington, ‘The triple bottom line for 21st century business’, *Earthscan Read. Bus. Sustain. Dev.*, pp. 20–43, Jan. 2001.
- [4] Silvaris Corporation, ‘The Current State of the OSB Market in 2021’, Jul. 25, 2021. <https://www.silvaris.com/the-current-state-of-the-osb-market-in-2021/> (accessed Aug. 19, 2021).
- [5] D. E. Kline, ‘Gate-to-Gate Life-Cycle Inventory of Oriented Standboard Production’, *Wood Fiber Sci.*, vol. 37, no. Corrim Special Issue, pp. 74–84, 2005.
- [6] F. Yapici, ‘Experimental Study on Combustion Properties and Thermo-Gravimetric Analyses of Oriented Strand Board (OSB)’, *Drv. Ind.*, vol. 71, no. 1, pp. 55–60, Mar. 2020, doi: 10.5552/drvind.2020.1909.
- [7] M. A. Dietsberger and L. E. Hasburgh, ‘Wood Products: Thermal Degradation and Fire’, in *Reference Module in Materials Science and Materials Engineering*, Elsevier, 2016, p. B9780128035818033000. doi: 10.1016/B978-0-12-803581-8.03338-5.
- [8] S. M. Cramer and R. H. White, ‘Fire performance issues’, *Wood Eng. 21st Century Res. Needs Goals Proc. Workshop Offer. Conjunction SEIASCE Struct. Congr. XV Portland Or. April 16 1997 Rest. VA Struct. Eng. Inst. Am. Soc. Civ. Eng. C1998*, pp. 75–86, 1997.
- [9] B. Meacham and M. McNamee, ‘Fire Safety Challenges of “Green” Buildings and Attributes’, Fire Protection Research Foundation, Shrewsbury, MA, FPRF-2020-13, Oct. 2020.
- [10] A. Sinha, J. A. Nairn, and R. Gupta, ‘Thermal degradation of bending strength of plywood and oriented strand board: a kinetics approach’, *Wood Sci. Technol.*, vol. 45, no. 2, pp. 315–330, May 2011, doi: 10.1007/s00226-010-0329-3.
- [11] D. B. McKeever, ‘Engineered wood products: a response to the changing timber resource’, *Pac. Rim Wood Mark. Rep.*, vol. 123, no. 5, p. 15, 1997.
- [12] R. M. Rowell, Ed., *Handbook of wood chemistry and wood composites*. Boca Raton, Fla: CRC Press, 2005.
- [13] R. Brandner, G. Flatscher, A. Ringhofer, G. Schickhofer, and A. Thiel, ‘Cross laminated timber (CLT): overview and development’, *Eur. J. Wood Wood Prod.*, vol. 74, no. 3, pp. 331–351, May 2016, doi: 10.1007/s00107-015-0999-5.
- [14] H. Gross, *Glulam Handbook Volume 1*. Stockholm, 2013.
- [15] J. Gil, ‘Performance of joints for glued laminated timber exposed to the ISO fire temperature curve’, Lund University, Lund, 2021. Accessed: Apr. 21, 2022. [Online]. Available: <http://lup.lub.lu.se/student-papers/record/9048812>
- [16] T. Sellers, *Plywood and Adhesive Technology*. CRC Press, 1985.
- [17] I. Andersen, G. R. Lundqvist, and L. Møhlhave, ‘Indoor air pollution due to chipboard used as a construction material’, *Atmospheric Environ. 1967*, vol. 9, no. 12, pp. 1121–1127, Jan. 1975, doi: 10.1016/0004-6981(75)90188-2.
- [18] R. L. Geimer, ‘Flake alignment in particleboard as affected by machine variables and particle geometry’, USDA Forest Service, Research Paper FPL 275, 1976.
- [19] R. A. Harris and J. A. Johnson, ‘Characterization of flake orientation in flakeboard by the von mises probability distribution function’, *Wood Fibre*, vol. 14, no. 4, pp. 254–266, 1982.

- [20] T. Nishimura, ‘Chipboard, oriented strand board (OSB) and structural composite lumber’, in *Wood Composites*, Elsevier, 2015, pp. 103–121. doi: 10.1016/B978-1-78242-454-3.00006-8.
- [21] G. Gunduz, F. Yapici, A. Ozcifici, and H. Kalaycioglu, ‘The Effects of Adhesive Ratio and Pressure Time on Some Properties of Oriented Strand Board’, *BioResources*, vol. 6, no. 2, pp. 2118–2124, 2011.
- [22] BS EN 300, *Oriented Strand Boards (OSB) – Definitions, classification and specifications*. British Standards Institution, 2006.
- [23] ISO, *Wood-based panels — Oriented strand board (OSB) — Definitions, classification and specifications*, 1st ed. Switzerland, 2009.
- [24] National Institute of Standards and Technology, *Performance Standard for Wood Structural Panels*. U.S. Department of Commerce, 2019.
- [25] Standards Council of Canada, *Construction sheathing (NIST PS 2-18, MOD)*. 2021.
- [26] R. H. White and J. E. Winandy, ‘Fire Performance of Oriented Strandboard’, presented at the Seventeenth Annual BCC Conferences on Flame Retardancy, 2006.
- [27] P. Rantuch, D. Kačíková, J. Martinka, and K. Balog, ‘The influence of heat flux density on the thermal decomposition of OSB’, *Acta Fac. Xylologiae Zvolen*, no. 57(2), 2015, doi: 10.17423/afx.2015.57.2.13.
- [28] M. A. Dietenberger, ‘Ignitability of materials in transitional heating regimes’, Svolen, Slovakia, Apr. 2004, pp. 31–41. [Online]. Available: <https://www.fs.usda.gov/treearch/pubs/7018>
- [29] M. A. Dietenberger and O. Grexa, ‘Correlation of smoke development in room tests with cone calorimeter data for wood products’, Slovak Republic, May 2000, pp. 45–55. Accessed: Aug. 19, 2021. [Online]. Available: <https://www.fs.usda.gov/treearch/pubs/5714>
- [30] O. Grexa, M. Jenessens, R. White, and M. A. Dietenberger, ‘Fundamental Thermophysical properties of materials derived from the cone calorimeter measurements’, presented at the 3rd International Scientific Conference on Wood and Fire Safety, Slovakia, 1996.
- [31] J. Ira, L. Hasalová, V. Šálek, M. Jahoda, and V. Vystrčil, ‘Thermal Analysis and Cone Calorimeter Study of Engineered Wood with an Emphasis on Fire Modelling’, *Fire Technol.*, vol. 56, no. 3, pp. 1099–1132, May 2020, doi: 10.1007/s10694-019-00922-9.
- [32] ASTM E1131-08, ‘Test Method for Compositional Analysis by Thermogravimetry’, ASTM International, West Conshohocken, PA, 2008. doi: 10.1520/E1131-08.
- [33] J. Gong, H. Zhu, H. Zhou, and S. I. Stolarov, ‘Development of a pyrolysis model for oriented strand board. Part I: Kinetics and thermodynamics of the thermal decomposition’, *J. Fire Sci.*, vol. 39, no. 2, pp. 190–204, Mar. 2021, doi: 10.1177/0734904120982887.
- [34] P. Reszka and J. L. Torero, ‘Fire Behavior of Timber and Lignocellulose’, in *Lignocellulosic Fibers and Wood Handbook*, N. Belgacem and A. Pizzi, Eds. Hoboken, NJ, USA: John Wiley & Sons, Inc., 2016, pp. 553–581. doi: 10.1002/9781118773727.ch22.
- [35] W. Sonderegger and P. Niemz, ‘Thermal conductivity and water vapour transmission properties of wood-based materials’, *Eur. J. Wood Wood Prod.*, vol. 67, no. 3, pp. 313–321, Aug. 2009, doi: 10.1007/s00107-008-0304-y.
- [36] Ł. Czajkowski, W. Olek, J. Weres, and R. Guzenda, ‘Thermal properties of wood-based panels: thermal conductivity identification with inverse modeling’, *Eur. J. Wood Wood Prod.*, vol. 74, no. 4, pp. 577–584, Jul. 2016, doi: 10.1007/s00107-016-1021-6.
- [37] O. Vololonirina, M. Coutand, and B. Perrin, ‘Characterization of hygrothermal properties of wood-based products – Impact of moisture content and temperature’, *Constr. Build. Mater.*, vol. 63, pp. 223–233, Jul. 2014, doi: 10.1016/j.conbuildmat.2014.04.014.

- [38] R. Igaz, L. Krišťák, I. Ružiak, M. Gajtanska, and M. Kučerka, ‘Thermophysical Properties of OSB Boards versus Equilibrium Moisture Content’, *BioResources*, vol. 12, no. 4, Art. no. 4, Sep. 2017, doi: 10.15376/biores.12.4.8106-8118.
- [39] G. Chen and B. He, ‘Stress-strain Constitutive Relation of OSB under Axial Loading: An Experimental Investigation’, *BioResources*, vol. 12, no. 3, pp. 6142–6156, Jul. 2017, doi: 10.15376/biores.12.3.6142-6156.
- [40] D. W. Green, J. E. Winandy, and D. E. Kretschmann, ‘Wood handbook-wood as an engineering material’, U.S. Department of Agriculture, Forest Service, Forest Products Laboratory, Madison, WI, General technical report FPL-GTR-113, 1999.
- [41] P. Bekhta, J. Lecka, and Z. Morze, ‘Short-term effect of the temperature on the bending strength of wood-based panels’, *Holz Als Roh- Werkst.*, vol. 61, no. 6, pp. 423–424, Dec. 2003, doi: 10.1007/s00107-003-0423-4.
- [42] ‘HFM 446 Lambda Series – Heat Flow Meter for Testing Insulation Materials’. Netzch.
- [43] ASTM E1354 – 17, ‘Test Method for Heat and Visible Smoke Release Rates for Materials and Products Using an Oxygen Consumption Calorimeter’, ASTM International, 2017. doi: 10.1520/E1354-17.
- [44] BS ISO 5660-1, *Reaction-to-fire tests. Heat release, smoke production and mass loss rate*. British Standards Institution, 2021.
- [45] M. M. Khan, A. Tewarson, and M. Chaos, ‘Combustion Characteristics of Materials and Generation of Fire Products’, in *SFPE Handbook of Fire Protection Engineering*, M. J. Hurley, D. Gottuk, J. R. Hall, K. Harada, E. Kuligowski, M. Puchovsky, J. Torero, J. M. Watts, and C. Wieczorek, Eds. New York, NY: Springer New York, 2016, pp. 1143–1232. doi: 10.1007/978-1-4939-2565-0_36.
- [46] *COMSOL Multiphysics®*. Stockholm, Sweden: COMSOL AB. [Online]. Available: <https://www.comsol.com>
- [47] V. K. R. Kodur and T. Z. Harmathy, ‘Properties of Building Materials’, in *SFPE Handbook of Fire Protection Engineering*, M. J. Hurley, D. Gottuk, J. R. Hall, K. Harada, E. Kuligowski, M. Puchovsky, J. Torero, J. M. Watts, and C. Wieczorek, Eds. New York, NY: Springer New York, 2016, pp. 277–324. doi: 10.1007/978-1-4939-2565-0_9.
- [48] *Eurocode 5 – Design of Timber Structures – Part 1-2: General – Structural Fire Design*. 2004.
- [49] C. Lautenberger, C. L. Tien, K. Y. Lee, and A. J. Stretton, ‘Radiation Heat Transfer’, in *SFPE Handbook of Fire Protection Engineering*, M. J. Hurley, D. Gottuk, J. R. Hall, K. Harada, E. Kuligowski, M. Puchovsky, J. Torero, J. M. Watts, and C. Wieczorek, Eds. New York, NY: Springer New York, 2016, pp. 102–137. doi: 10.1007/978-1-4939-2565-0_4.
- [50] V. Babrauskas, ‘The Cone Calorimeter’, in *SFPE Handbook of Fire Protection Engineering*, M. J. Hurley, D. Gottuk, J. R. Hall, K. Harada, E. Kuligowski, M. Puchovsky, J. Torero, J. M. Watts, and C. Wieczorek, Eds. New York, NY: Springer New York, 2016, pp. 952–980. doi: 10.1007/978-1-4939-2565-0_28.
- [51] E. Mikkola and I. S. Wichman, ‘On the Thermal Ignition of Combustible Materials’, *Fire Mater.*, vol. 14, pp. 87–96, 1989.

11 Appendices

11.1 Declaration of Performance of the Testing Specimen

Declaration of performance acc. Regulation EU No. 305/2011 (CPR)
No. OSB3-CPR-2013-07-01-8 - OSB 3 ECO



SIA „KRONOSPAN Rīga”
Daugavgrīvas soseja 7B, Rīga, LV-1016, Latvia
Tel.: +371 67 430 147, Fax: +371 67 430 167
Id. N°: 40003774690, VAT N°: LV40003774690
office@kronospan-riqa.lv, www.kronospan-express.com

DECLARATION OF PERFORMANCE No. OSB3-CPR-2013-07-01-8

- Unique identification code of the product-type:
OSB 3 ECO
- Intended use or uses of the construction product:
**For internal use as a structural component in humid conditions
(OSB/3 acc. EN 300 is load-bearing boards for use in humid conditions)**
- Name and contact address of the manufacturer:
**SIA "KRONOSPAN Rīga"
Daugavgrīvas soseja 7B, LV-1016, Rīga, Latvia
Business ID 40 003 774 690
www.kronospan-express.com**
- System of assessment and verification of constancy of performance:
System 2+
- Harmonised standard:
EN 13986:2004 + A1:2015
- The notified factory production control certification body:
**Fraunhofer-Institute for Wood Research
Wilhelm-Klauditz-Institute WKI
Bienroder Weg 54 E, 38108 Braunschweig, Germany
Notified body no. 0765**

The notified factory production control certification body- **Wilhelm-Klauditz-Institute WKI, Germany** - performed initial inspection of the manufacturing plant and of factory production control and performs continuous surveillance, assessment and evaluation of factory production control under the system 2+ as described in harmonised standard **EN 13986:2004+A1:2015**.

Notified body issued the certificate of conformity of the factory production control No. **0765-CPR-778**

- Declared performance

Specification		Performance				Harmonised technical specification
		Boards thickness in mm				
		9 – 10 mm	> 10 – 18	> 18 - 25	> 25 - 30	
Bending strength acc. EN 310	Major axis	22 MPa	20 MPa	18 MPa	16 MPa	Technical class OSB/3 acc. to EN 300
	Minor axis	11 MPa	10 MPa	9 MPa	8 MPa	
Bending stiffness (Modulus of elasticity) acc. EN 310	Major axis	3500 MPa	3500 MPa	3500 MPa	3500 MPa	
	Minor axis	1400 MPa	1400 MPa	1400 MPa	1400 MPa	

Essential characteristics			Performance				Harmonised technical specification
			Boards thickness in mm				
			9 – 10	> 10 – 18	> 18 - 25	> 25 - 30	
1			2	3	4	5	6
Strength acc. EN 12369-1 [N/mm ²]	Bending f_m	Major axis (0)	18,0	16,4	14,8	NPD	EN 13986:2004+ A1:2015
		Minor axis (90)	9,0	8,2	7,4	NPD	
	Tension f_t	Major axis (0)	9,9	9,4	9,0	NPD	
		Minor axis (90)	7,2	7,0	6,8	NPD	
	Compression f_c	Major axis (0)	15,9	15,4	14,8	NPD	
		Minor axis (90)	12,9	12,7	12,4	NPD	
	Panel shear f_v		6,8	6,8	6,8	NPD	
	Planar shear f_p		1,0	1,0	1,0	NPD	

Declaration of performance acc. Regulation EU No. 305/2011 (CPR)
No. OSB3-CPR-2013-07-01-8 - OSB 3 ECO

7		2	3	4	5	6		
Stiffness (MOE) acc. EN 12369-1 [N/mm ²]	Bending E _m	Major axis (0)	4930		NPD	EN 13986:2004 + A1:2015		
		Minor axis (90)	1980		NPD			
	Tension E _t	Major axis (0)	3800		NPD			
		Minor axis (90)	3000		NPD			
	Compression E _c	Major axis (0)	3800		NPD			
		Minor axis (90)	3000		NPD			
Panel shear G _v		1080		NPD				
Planar shear G _r		50		NPD				
Punching shear as point load strength and point load stiffness		NPD						
Racking resistance		NPD						
Impact resistance		Pass						
Reaction to fire acc. EN 13501-1		class D-s2,d0 ¹ for th. 9 till 30 mm class D-s1,d0 ² for th. 30 mm						
Water vapour permeability		NPD						
Content of formaldehyde		Class E1 (≤ 0.3 mg/ 100g oven dry board)						
Release (content) of pentachlorophenol (PCP)		<0,1 mg/kg						
Airborne sound insulation acc. EN 13986		NPD						
Sound absorption acc. EN 13986, Tab.10		NPD						
Thermal conductivity (density) acc. EN 12664		NPD						
Embedment strength		NPD						
Air permeability		NPD						
Durability	Board thickness [mm]		9 – 10	> 10 – 18	> 18 – 25	> 25 – 30		
	Internal bond acc. EN 319		0,34 MPa	0,32 MPa	0,30 MPa	0,29 MPa		
	Swelling in thickness (24h) acc. EN 317		15 %	15 %	15 %	15 %		
	Moisture resistance (Internal bond after boil test) acc. EN 1087-1		0,15 MPa	0,13 MPa	0,12 MPa	0,06 MPa		
	Mechanical	Modification factor k _{mod} acc. EN1995-1-1, tab.3.1.	Service class	Permanent load	Long-term load	Medium-term load	Short-term load	Instantaneous load
			1	0,40	0,50	0,70	0,90	1,10
		2	0,30	0,40	0,55	0,70	0,90	
	Modification factor k _{def} acc. EN 1995-1-1, tab. 3.2		k _{def} = 1,50 (service class 1) k _{def} = 2,25 (service class 2)					
	Biological durability acc. EN335		use class 2					

¹ Reaction to fire classification is valid for following end use conditions: product with a closed or an open air gap not more than 22mm behind the product. The reverse face of the cavity shall be at least class A2-s1,d0 products with minimum density 10 kg/m³.

² Reaction to fire classification is valid for following end use conditions: product without substrate or fixed directly on any substrate of reaction to fire class at least D-s1,d0.

8. The performance of the product identified in point 1 is in conformity with the declared performance in point 7.

This declaration of performance is issued under the sole responsibility of the manufacturer identified in point 3.

Signed for and on behalf of the manufacturer by:

..... Janina Mitrofanova
 Member of the Board

..... Ivars Plaudis
 Technical Director / Procurist

Riga, 16.04.2018